Bioconjugate Chemistry

Article

Theranostic nanocages for imaging and photothermal therapy of prostate cancer cells by active targeting of neuropeptide-Y receptor

Svetlana Avvakumova, Elisabetta Galbiati, Laura Sironi, Silvia A. Locarno, Luca Gambini, Chiara Macchi, Laura Pandolfi, Massimiliano Ruscica, Paolo Magni, Maddalena Collini, Miriam Colombo, Fabio Corsi, Giuseppe Chirico, Sergio Romeo, and Davide Prosperi

Bioconjugate Chem., **Just Accepted Manuscript** • DOI: 10.1021/acs.bioconjchem.6b00568 • Publication Date (Web): 03 Nov 2016

Just Accepted

ACS Publications

Bioconjugate Chemistry is published by the American Chemical Society. 1155 Sixteenth Street N.W., Washington, DC 20036

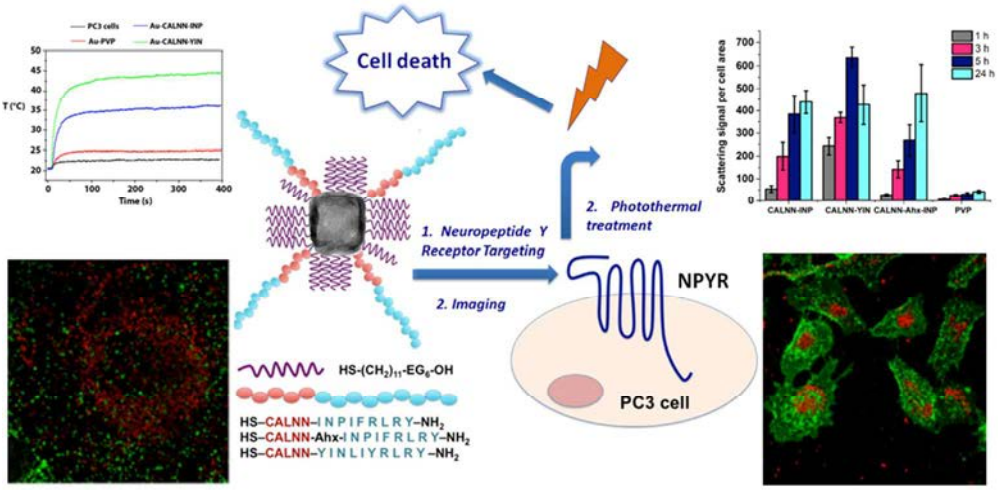

TOC graphic

85x42mm (300 x 300 DPI)

Theranostic Nanocages for Imaging and Photothermal Therapy of Prostate Cancer Cells by Active Targeting of Neuropeptide-Y Receptor

*Svetlana Avvakumova,[1] Elisabetta Galbiati,[1] Laura Sironi,[2] Silvia A. Locarno,[3] Luca Gambini,[3] Chiara Macchi,[4] Laura Pandolfi,[1] Massimiliano Ruscica,[4] Paolo Magni,[4] Maddalena Collini,[2] Miriam Colombo,[1] Fabio Corsi,[5] Giuseppe Chirico,[2] Sergio Romeo,[3] and Davide Prosperi[1,]**

[1] NanoBioLab, Dipartimento di Biotecnologie e Bioscienze e Centro di Nanomedicina, Università di Milano-Bicocca, Piazza della Scienza, 2, 20126, Milano, Italy. [2] Dipartimento di Fisica e Centro di Nanomedicina, Università di Milano-Bicocca, Piazza della Scienza 3, 20126, Milano, Italy. [3] Università degli Studi di Milano, Dipartimento di Scienze Farmaceutiche, via Mangiagalli 25, 20133 Milano, Italy. [4] Università degli Studi di Milano, Dipartimento di Scienze Farmacologiche e Biomolecolari, via Balzaretti 9, 20133 Milano, Italy. [5] Surgery Department, Breast Unit, ICS Maugeri S.p.A. SB, via S. Maugeri 10, 27100 Pavia, Italy.

Email: davide.prosperi@unimib.it

KEYWORDS: Neuropeptide Y; gold nanocages; theranostics; molecular imaging; photothermal treatment; prostate cancer

ABSTRACT: Gold nanocages (AuNCs) have been shown to be a useful tool for harnessing imaging and hyperthermia therapy of cancer, thanks to their unique optical properties, low toxicity and facile surface functionalization. Herein, we use AuNCs for selective targeting of prostate cancer cells (PC3) via specific interaction between neuropeptide Y (NPY) receptor and three different NPY analogs conjugated to AuNCs. Localized surface plasmon band of the nanoconjugates was set around 800 nm, which is appropriate for in vivo applications. Long-term stability of nanoconjugates in different media was confirmed by UV-vis and DLS studies. Active NPY receptor targeting was observed by confocal microscopy showing time-dependent AuNCs cellular uptake. Activation of ERK1/2 pathway was evaluated by Western blot to confirm the receptor-mediated specific interaction with PC3. Cellular uptake kinetics were compared as a function of peptide structure. Cytotoxicity of nanoconjugates was evaluated by MTS and Annexin V assays, confirming their safety within the concentration range explored. Hyperthermia studies were carried out irradiating the cells, previously incubated with AuNCs, with a pulsed laser at 800 nm wavelength, showing a heating enhancement ranging from 6 to 35 °C above the culture temperature dependent on the irradiation power (between 1.6 and 12.7 W/cm2). Only cells treated with AuNCs underwent morphological alterations in the cytoskeleton structure upon laser irradiation, leading to membrane blebbing and loss of microvilli associated to cell migration. This effect is promising in view of possible inhibition of proliferation and invasion of cancer cells. In summary, our Au-peptide NCs proved to be an efficient theranostic nanosystem for targeted detection and activatable killing of prostate cancer cells.

INTRODUCTION

A great challenge in modern oncology resides in the detection, localization and treatment of tumor neoplasms, especially at early stages of development. Among different conventional strategies used to selectively target cancer cells, monoclonal antibodies have become a magic bullet.[1,2] However, numerous drawbacks in antibody treatments have appeared with time, including poor pharmacokinetics and biodistribution as well as compromised functionality of the immune system,[3] making this solution more complicated than expected.[4] As an alternative to the use of antibodies, synthetic peptides reminiscent of those naturally occurring in the human organism, so called regulatory peptides, are gaining increasing interest in cancer research.[5] Short peptides can be easily synthesized using automated synthesizers and their pharmacokinetic profiles can be improved by making appropriate changes in the peptide sequence. Regulatory peptides include brain neuropeptides, gut peptide hormones, vasoactive peptides, and peptides of the endocrine system, and act on multiple targets in the human body modulating the function of most key organs and metabolic processes.[6] More recently, these regulatory peptides have been suggested as powerful small ligands for cancer targeting, as several peptide receptors were found overexpressed in certain tumors, and indicated for use as markers for localization of tumors and of their metastases.[7] Actually, advanced clinical diagnosis of cancer takes advantage of molecular receptor targeting by radiolabeled peptides.[3,8] The major challenge for radiolabeling is to find a compromise between peptide and radionuclide dosages: a minimum amount of peptide is needed to reduce any adverse pharmacologic effects, while high specific radioactivity is crucial for optimal resolution. On the other hand, the potential of nuclear imaging techniques (PET, SPECT) is limited by the cost of radionuclides with short half-lives and relatively poor

resolution. In the last decade, great efforts have been made to develop new kinds of imaging agents taking advantage of the progress made by nanoparticle research.[9] Among myriads of nanoparticles, gold nanocages (AuNCs), versatile nanostructures characterized by hollow interiors and ultrathin porous walls, have attracted a great attention thanks to their unique optical properties associated to a tunable localized surface plasmon resonance (LSPR).[10] The two- and three-photon luminescence capabilities and strong optical absorption of AuNCs allow labeling and quantitatively tracking the cells using two-photon and photoacoustic microscopy, therefore providing valid alternative to radiolabeling.[11,12,13] In addition, AuNCs have been used as promising agents for noninvasive photothermal therapy taking advantage of the large absorption cross-section in the near infrared (NIR) region of the optical spectrum.[14,15] More recently gold nanoparticles have been shown to display substantial Joule heating under radiofrequency fields, opening up their application in MRI therapy,[16,17] though the mechanisms and efficiency of this effect is still under debate. Finally, the easy functionalization of AuNCs with thiol-containing molecules through Au-S covalent interaction make them excellent nanoconjugates for use as tumor targeting agents. Combined together, these features give rise to an efficient multifunctional nanotheranostics able to label and detect tumor cells via specific targeting of molecular receptors and to induce their irreversible death through NIR-assisted hyperthermia.[18,19,20]

Despite the remarkable progress in the field of small peptides as targeting agents, the exploration of new peptide receptors overexpressed preferentially by human cancers remains an attractive goal in order to optimize the therapeutic possibilities toward a personalized cure. In this context, neuropeptides play a crucial role being not only potent cellular growth factors in normal cells, but also responsible for autocrine/paracrine stimulation of tumor cell proliferation

and migration.[5] Neuropeptide Y (NPY) is a 36 amino acid peptide that acts as a neurotransmitter and neuromodulator and, in humans, exerts its effect through a family of four G-protein coupled receptors, namely, Y1, Y2, Y4, and Y5. In particular, the expression of Y1, Y2, and Y5 receptors is associated with different stages of either carcinogenesis or tumor progression.[5] Recent studies by Magni *et al.* explored the expression of Y1-R gene in prostate cancer cells and the role of NPY in regulating tumor growth.[21] However, the attention has been mostly focused on GPCR itself so far, while the data regarding NPY receptor (NPYR) targeting in prostate cancer are still lacking. Aiming to explore the potential of NPYR targeting in the treatment of prostate cancer, we prepared gold nanocages functionalized with three short peptides – derivatives of NPY – specific to NPYR (Y1/Y2). These Au-peptide nanocages were first assessed in terms of targeting efficiency in PC3 prostate cancer cells. Next, the nanoconjugates were exploited as probes for confocal microscopy and as heating mediators for light-triggered cancer thermotherapy, taking advantage of the theranostic character of AuNCs (Figure 1).

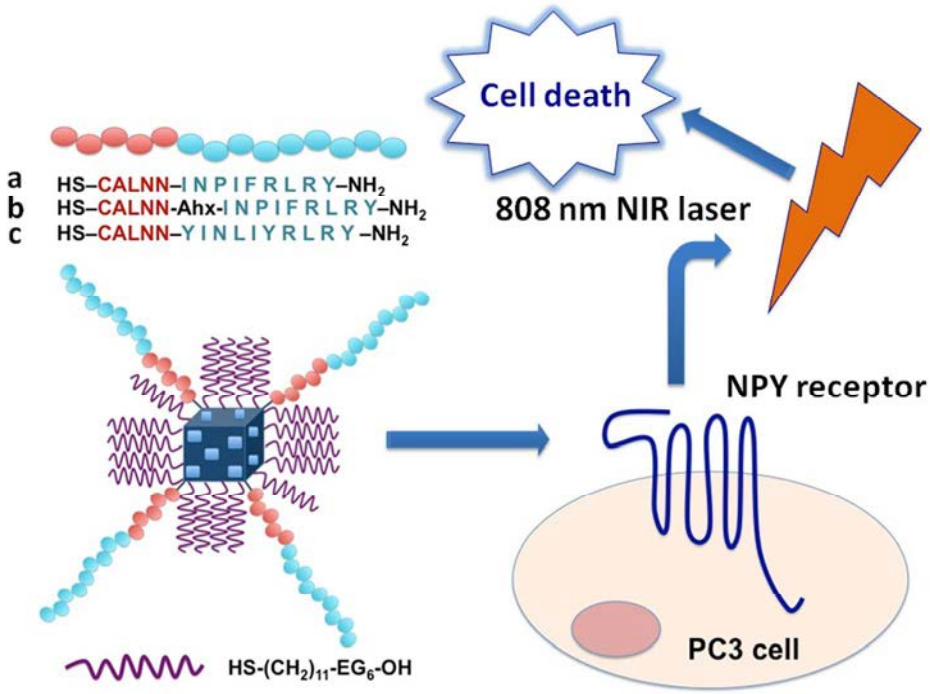

Figure 1. Schematic representation of NPYR targeting on prostate cancer cells by peptide-functionalized gold nanocages and subsequent hyperthermia by NIR irradiation. Three kinds of AuNCs are considered, deriving from the surface functionalization with selected peptides, namely a) Au-CALNN-INP, b) Au-CALNN-Ahx-INP, c) Au-CALNN-YIN, respectively. Peptide sequences are sketched in the figure. The available surface of AuNCs was saturated by short PEG molecules, HS-(CH2)11-EG6-OH.

RESULTS AND DISCUSSION

Design and synthesis of peptides. The rationale of peptide design was based on the following issues: 1) preservation of the native alpha-helical conformation of NPY, essential for the NPYR recognition, and 2) successful conjugation of the peptides to AuNCs giving stable nanoparticles without compromising the receptor recognition ability. Peptide structures, reported in Figure 1, contain a nanoparticle-binding motif (CALNN) and a NPY-binding motif. NPY-binding motifs were synthesized according to the results of the studies reported previously.[22] CALNN pentapeptide, successfully used by Levy *et al.* to favor an ordered peptide assembly on the nanoparticle surface, was introduced as a linker for AuNCs stabilization via Au-thiol bond of terminal Cys.[23] As for NPYR binding part, the binding motifs were derived from the *C*-terminus NPY 25-36 fragment - common recognition site for the receptor binding conserved in all of the ligands.[24] In brief, the amidated *C*-terminus as well as the Arg33 and Arg35 residues were conserved for their importance in maintaining the NPYR binding. As for CALNN-INP, Leu30 was exchanged with Pro in order to increase the fragment activity since the turn-inducing sequence Asn29-Pro30 stabilizes the essential helix conformation. To improve the segment helicity, Gln34 was also substituted with Leu in all three peptides, while Thr32 was exchanged

with aromatic amino acids like Phe or Tyr to increase the peptide-receptor interaction.[25] In CALNN-Ahx-INP, 6-aminohexanoic acid (Ahx) was introduced between the nanoparticle-binding motif and the NPY-binding motif for two reasons: 1) to study how the sequence CALNN could influence the stability of the peptide secondary structure when it is directly or not linked to the receptor-binding motif; 2) to study possible effects of an elongation and separation of the receptor-binding motif from nanoparticle surface on the targeting efficiency of the nanoconjugate. Peptides were synthesized manually by Fmoc-strategy using the Rink Amide resin, purified by a preparative HPLC and characterized by analytical HPLC. The identity and purity were confirmed by UPLC mass spectrometry. The peptide secondary structure was studied by circular dichroism (CD). The CD spectra, shown in the Figure S1, were performed in phosphate buffer saline (PBS)/TFE 70:30 (10 μM solutions) in the far-UV region (190-250 nm). As expected, in the case of CALNN-INP and CALNN-YIN, the double minima at 208 and 222 nm and the positive band below 200 nm indicate the presence of a well-defined helical structure. The percentage of α-helix in the peptides was calculated with DICHROWEB[26] using K2d method,[27] which estimated a value of 56% and 55% respectively. Then, the presence of Pro in position 30 allowed to maintain the helical secondary structure also with a shorter sequence. In CALNN-Ahx-INP, the typical bands of α-helix structure disappeared (only 28% calculated with DICHROWEB), but it exhibited a negative band at 218 nm and a positive band at 193 nm, typical of an antiparallel β-pleated sheets. These results suggested that the pentapeptide CALNN could be considered useful not only for the assembly on the nanoparticle surface, but also for the stabilization of the helical structure when it is directly linked to the peptide receptor-binding motif.

Nanoparticle synthesis and functionalization. PVP-coated AuNCs of 40.8 ± 1.8 nm were prepared by well-described galvanic replacement using silver nanocubes as substrates (Figure 2, a-c).[28,29] To prepare the three different batches of functionalized AuNCs, as-synthesized nanoparticles were reacted with a mixture of each peptide type and thiolated PEG to allow for capping-ligand exchange and Au-S bond formation. As above mentioned, the CALNN sequence was used as a spacer between AuNC surface and the targeting moiety. CALNN peptide allowed keeping the colloidal stability of nanoconjugates by stabilization of the targeting peptide structure and its interaction with the charged nanoparticle surface.[23] As discovered by Levy *et al*., thanks to the presence of alanine and leucine in positions 2 and 3 promoting the self-assembly of the peptide through intermolecular hydrophobic interactions, CALNN peptide is able to form a self-assembled monolayer on gold nanoparticles, donating to nanoparticles extremely stable properties.[30]

AuNC functionalization resulted in a large shift of UV-Vis plasmon absorption from 802 to 860 nm, characteristic of the dielectric constant change due to peptide and PEG conjugation to the particle surface (Figure 2d). This was also confirmed by changes in electrokinetic and size-distribution features of nanoparticles determined by DLS and zeta-potential analyses. The hydrodynamic size of the nanoconjugates slightly increased, while their zeta-potential values became less negative compared to non-functionalized nanocages (see Table 1). The peptide amount per particle was evaluated by UV-vis spectroscopy on washing supernatant by subtracting a reference blank obtained as a mixture of PEG and dimethylsulfoxide at the same amounts and conditions of the reaction. On average, we found around 2000 peptide molecules per particle (Table 1). The long-term colloidal stability was monitored by DLS and zeta-potential measurements for several months after peptide conjugation, (Figure S2). The nanoparticles were

highly stable in mQ water as monitored by UV-vis spectroscopy and after incubation in different buffer solutions, including acetate buffer (pH 4.5), 20 mM HEPES (pH 7.8), 2.5 mM NaCl (pH 2 and pH10) and fetal bovine serum (FBS) (Figure S3, a-c). Surprisingly, all nanoconjugates were found to be stable both in 100% FBS and in acidic sodium chloride solution (pH 2), as confirmed by the very slight changes in the position and intensity of the plasmonic band. Halas *et al*. have investigated the stability of Ag-Au hollow nanospheres across a range of different pH and in human serum at physiological pH.[24] Disappointingly, the authors noticed that the structural integrity of the hollow architecture was compromised both in serum and in strongly acidic pH causing the *in vivo* degradation of AuNCs.

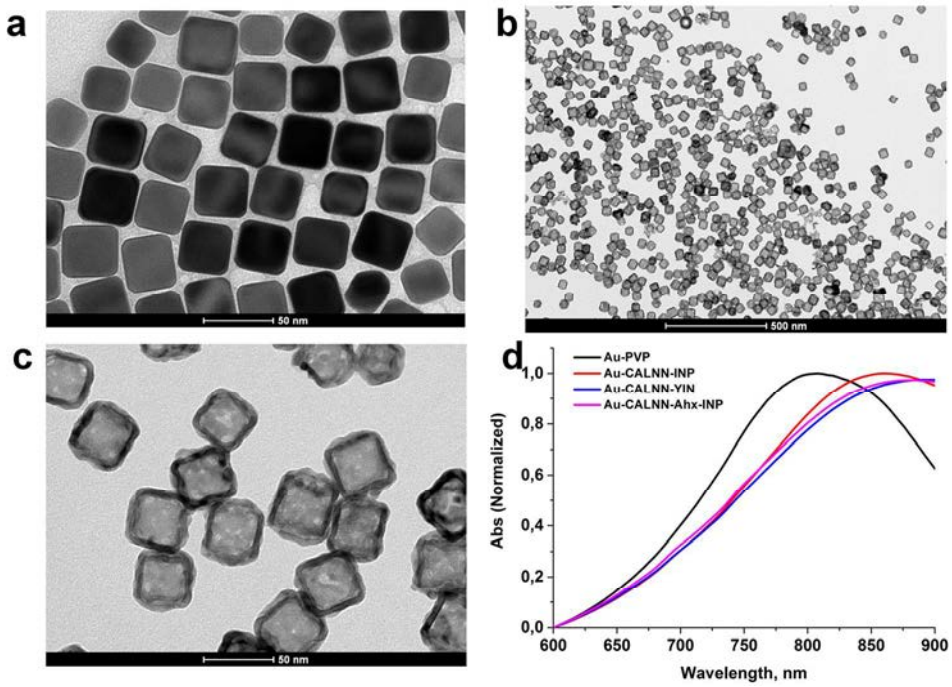

Figure 2. a) TEM micrographs of as-prepared silver nanocubes - medium size 34.7 ± 2.5 nm (scale bar 50 nm); b) TEM micrographs of as-prepared Au-PVP NCs (scale bar 500 nm); c) TEM micrographs of as-prepared Au-PVP NCs – medium size 40.8 ± 1.8 nm (scale bar 50 nm); d) UV-vis spectra of AuNCs before and after functionalization with peptides.

This effect was attributed to the presence of Ag on the inner surface of the nanoparticles leading to oxidation and consequent alteration of the integrity of the particles. In contrast, the structural integrity of our AuNCs was maintained in FBS, and no silver leakage was observed by TEM analysis. This improved stability is attributable to the presence of Au layers both inside and outside the cage walls, protecting them from oxidation and making them stable under the aggressive biological conditions (Figure S3).[25] Moreover, a careful design of the ligand shell to protect the nanoparticles from aggregation, using both CALNN pentapeptide and PEG at right proportion, has contributed to the particle stability even at harsh conditions.[30]

Table 1. Hydrodynamic size (DLS), zeta-potential and ligand shell composition of nanoparticles: 1 - Au-PVP, 2 - Au-CALNN-INP, 3 - Au-CALNN-YIN, 4 - Au-CALNN-Ahx-INP.

N°	Hydrodynamic size, nm	Zeta-potential, mV	peptide/NP
1	44.25 ± 13.45, PDI 0.154	–32.7 ± 4,20	–
2	45.56 ± 12.87, PDI 0.189	–5.66 ± 7.47	2.04×10^3
3	51.92 ± 14.27, PDI 0.160	–4.80 ± 5.62	1.67×10^3
4	50.04 ± 17.51, PDI 0.225	–4.11 ± 3.98	2.50×10^3

NPYR targeting. A nanoconjugate drug or diagnostic agent with potential impact in the clinics should have a distinct capacity to target the disease *in-situ*. Either passive or active targeting have been explored in details so far. Besides the "enhanced permeability and retention" (EPR) effect, passive targeting largely exploits also intrinsic physico-chemical characteristics of nanoparticles, including charge, size, shape and material composition.[31] For example, cationic nanoparticles electrostatically bind to negatively charged phospholipid head-groups exposed on the cell surface, while lipid nanoparticles can fuse with the cell membrane and enter the cell without involving the interaction with any specific receptor.[32,33] On the other hand, active targeting requires the interaction between a conjugated targeting ligand and a molecular receptor,

preferentially a protein or a carbohydrate molecule or cluster, overexpressed on the outer surface of the cell.[34] Competitive binding or using scrambled peptides (or nonspecific antibodies) are two major approaches to characterize the active targeting efficiency of functionalized nanoparticles. In the first approach, targeted particles are incubated with receptor-positive cells in the presence of large (usually 10 to 100-fold) excess of free ligand, so that nanoparticle binding is initially hampered by the receptor saturation.[35] In the second approach, peptides with randomly mixed amino acid sequences are used to show decreased binding efficiency of nanoparticles.[36] Both approaches have their advantages and disadvantages and thus multiple strategies should be used to assess specific receptor binding. Another approach, commonly used in molecular biology to study receptor-ligand interactions, includes the assessment of signal transduction activation upon receptor binding. Here we propose to use this approach to prove the specific molecular binding of nanoparticles to the cellular receptors, taking advantage of the intracellular biochemical events triggered by the receptor binding process. Once cells recognize targeting molecules on the nanoparticle surface, they respond to extracellular stimuli by engaging specific intracellular programs, including the signaling cascade that leads to the activation of regulatory sentinel genes, such as the mitogen-activated protein kinases (MAPKs). This chain of reactions, called intracellular signal transduction, allows signal to be transmitted from the cell surface to a variety of intracellular targets. We reasoned that the detection of the activation/deactivation of different downstream signals induced by the nanoparticle binding to the receptor could be a corroborating proof of the involvement of ligand-receptor active recognition compared to conventional assays. In other words, when peptide-conjugated nanoparticle binds to NPY receptor on PC3 cell, a signaling cascade activation takes place. In particular, we focused on the phosphorylation of the extracellular signal-regulated kinase (ERK),

which is a pivotal step of the cytosolic signaling pathway associated with NPYR activation. ERK belongs to the MAPK pathway, and its activation plays a key role in the signaling process leading to cell proliferation induced by growth factors that act through either protein-tyrosine kinase or G protein-coupled receptors.[37,38] Activation of ERK is mediated by the Raf/Ras/MEK pathway, where MEK activates members of the ERK family by phosphorylation of both threonine and tyrosine residues. Once activated, ERK phosphorylates a variety of targets, including other protein kinases and transcription factors.[39] Lee et al. reported that heregulin-functionalized nanorods binding to HER2 receptor could stimulate ERK phosphorylation in MCF7 breast cancer cells.[40] The increase in ERK phosphorylation was associated to the existence of "active zones," i.e., dynamic regions in the cell periphery, exhibiting higher rates of nanoparticle binding compared to the rest of the cell, suggesting, therefore, a localized receptor activation.

In our experiments, we first confirmed that the chemical modification of peptides required for AuNC conjugation did not compromise their ability to bind to the receptors. For this purpose, we analyzed ERK phosphorylation after incubation of PC3 cells with free peptides. All experimental conditions (peptide concentration, incubation time) were set up basing on our previous expertise.[21] All three peptides at 10^{-7} M concentration induced a significant level of ERK phosphorylation within 10 min (Figure 3). As we expected, the comparison between the shortest peptide under investigation, i.e., CALNN-INP, and its Ahx-modified analogue showed that the highest phosphorylation ratio (~%) was achieved with the short peptide associated with a good α-helix conformation. As for CALNN-YIN peptide, its pERK/ERK ratio of reached ~260-270% at 10^{-7} M peptide concentration. After 20 min incubation, pERK/ERK ratio decreases in all three cases, almost reaching control levels, which is indicative of short-term phosphorylation.

Next, in order to assess the downstream intracellular signaling upon nanoparticle binding, ERK phosphorylation was measured in PC3 cells targeted with peptide-conjugated AuNCs. Figure 3 shows that all Au-peptide NCs were indeed able to stimulate ERK activation, therefore confirming the occurrence of a specific interaction with NPYR. Generally, the response of ERK activation is both enhanced (~150%-250%) and prolonged (from 10 to 20 min) compared to the respective free peptides, depending on the peptide sequence. This effect was likely associated to the presence of the nanocage.

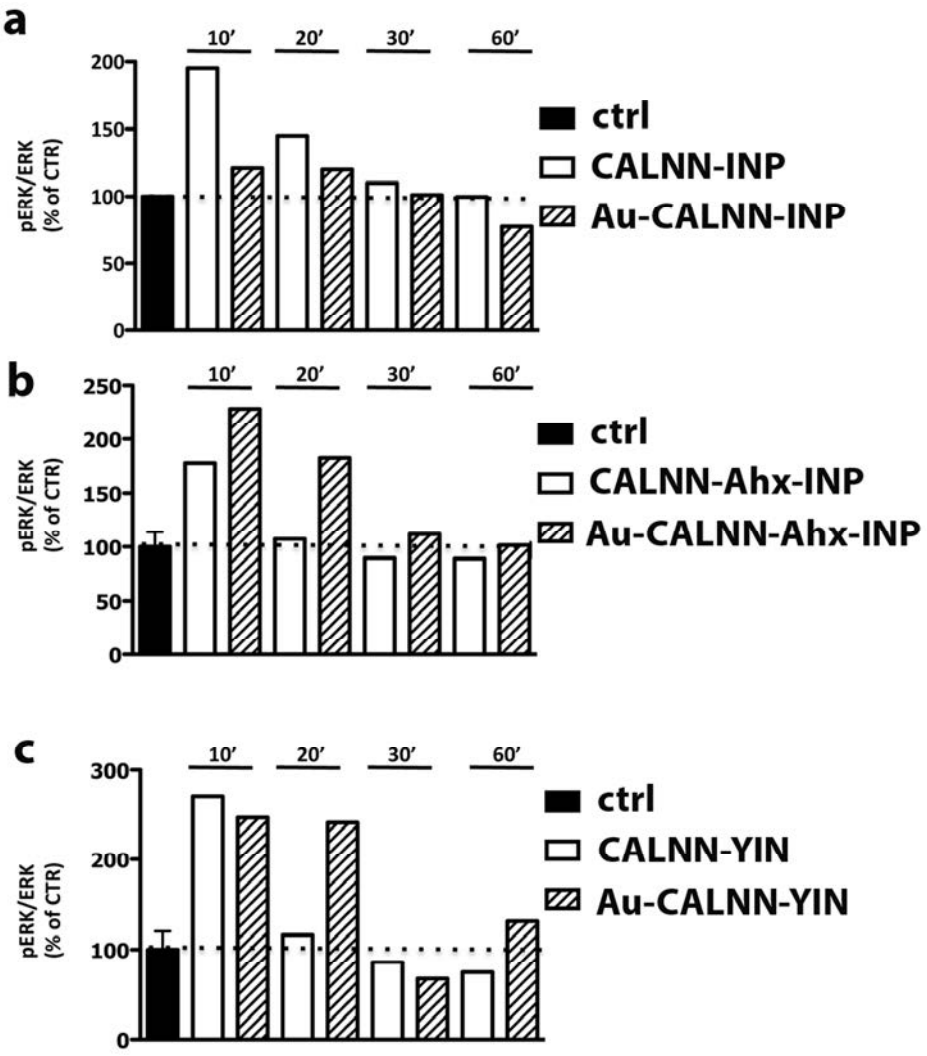

Figure 3. Time dependence of ERK phosphorylation in PC3 cells in response to specific NPYR targeting by nanocages decorated with a) CALNN-INP, b) CALNN-Ahx-INP, and c) CALNN-YIN peptides. Number of replicates, n = 3.

Indeed, multivalent interaction between peptides and receptors could take place due to higher ligand density on the particle surface leading to higher binding avidity. In addition, the distribution of peptide molecules on the nanoparticle surface was regular due to both CALNN and PEG contribution, leading to a more appropriate presentation of the peptide binding motif to the receptor interaction site.

Our findings are corroborated by previous evidence by Chan and co-workers that spherical gold nanoparticles conjugated with anti-HER2 antibody could firmly anchor on SK-BR-3 cell surface, resulting in prolonged receptor binding compared to the antibody alone.[40] The authors showed that nanoparticle size between 40-50 nm is critical to be internalized via receptor-mediated endocytosis, keeping a balance between multivalent cross-linking of membrane receptors and the process of membrane wrapping involved in clathrin polymerization required for the endosomal vesicle formation. We evaluated the influence of the peptide structure on the interaction with NPYR and, consequently, on ERK stimulation. All peptides showed high levels of phosphorylation compared to the control. Unexpectedly, the longer peptide CALNN-Ahx-INP, once bound to nanoparticle, showed even higher phosphorylation levels compared to its shorter analog, CALNN-INP, in contrast to the response of the peptide alone (Figure 3, a, b). Au-CALNN-YIN NPs confirmed their efficiency showing extremely high pERK/ERK ratios at short incubation time, and a prolonged effect up to 60 min after incubation (Figure 3c).

Assessment of AuNC uptake by confocal microscopy. Thanks to their unique optical absorption and scattering properties, gold nanoparticles, as small as 4 nm in size, can be detected

inside the cells by laser confocal scanning microscopy in scattering (reflective) mode, as reported by Rotello et al.[41] Also, larger anisotropic gold nanoparticles can be detected in living cells and followed in their intracellular dynamics.[42] In our study, we applied this technique to investigate the internalization kinetics of NPY-conjugated AuNCs into PC3 cells. As shown in Figure 4, the most part of peptide-conjugated nanoparticles were found either crossing the cellular membrane or inside the cells after 1 h of incubation. Quite surprisingly, Au-PVP nanocages missing the peptide ligand were hardly taken up by the cells (Figure S5), suggesting very high selectivity of peptide-mediated nanoconjugate internalization. As observed from histograms in Figure 4d and from the kinetic analysis (Figure S6), Au-CALNN-YIN NPs have the fastest internalization kinetics with growth time 3 ± 1 h, and shows an overshooting effect at about 5 h of incubation time with a subsequent relaxation time of about 24 ± 1 h. The kinetics of internalization of Au-CALNN-INP NPs shows a single growth component (Figure S6) with relaxation time = 3 ± 1 h. The growth kinetics of its longer analog is slower with growth time = 6 ± 1.3 h. Notably, after 24 h of incubation, the amount of Au nanocomposites internalized by the cells reached a basically common value among the three different Au-peptide nanocages. For a better understanding, full-size confocal microscopy images are reported in SI (Figure S4A-D).

These results are in line with the data from ERK-phosphorylation investigations, where the highest pERK/ERK ratio was attributed to Au-CALNN-YIN NPs, in fact, showing the fastest accumulation kinetics. The major cellular uptake, and, as a consequence, higher pERK level, could be attributed to higher affinity of YIN peptide sequence not only to Y1 receptor (ED_{50} = 9 nM), but also to Y2 receptor (IC50 = 8 nM), while INP peptide sequence was found to have affinity only to Y1 receptor subtype (IC50 = 10 nM versus IC50 = 480 nM for Y2 receptor).[43]

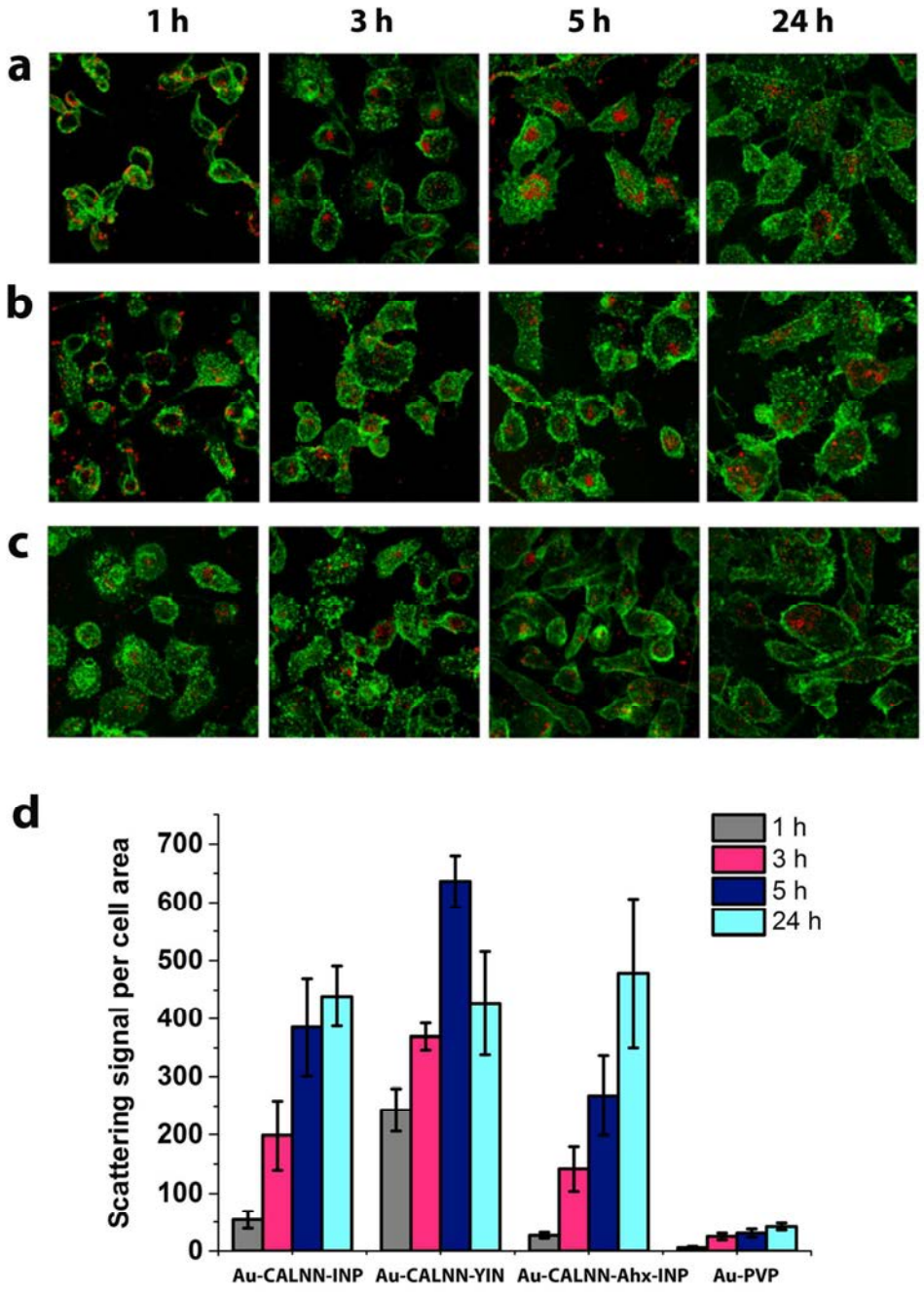

Figure 4. Confocal microscopy images (162 μm × 162 μm) of PC3 cells incubated with peptide-functionalized AuNCs: a) Au-CALNN-INP NPs; b) Au-CALNN-Ahx-INP NPs; c) Au-CALNN-YIN NPs. Cellular membranes are stained with AlexaFluor488–conjugated Wheat germ agglutinin (green), while AuNCs are visualized in reflection mode (red); d) Cellular uptake quantification by confocal microscopy. Scattering signal per cell area is reported after measuring

at least 50 cells per sample. The nanoparticle uptake, evaluated by summing the scattering signal from all the nanoparticles inside each cell normalized to the cell section area, was averaged over at least 50 cells.

Determination of nanoparticle uptake and trafficking by transmission electron microscopy. In order to get insight into the interaction between the nanoconjugates and the cellular environment, the nanocage trafficking pathway inside the cells was studied by TEM. PC3 cells were incubated with the particles for different periods of time (from 30 min to 48 h) at 37 °C, then washed, harvested and processed following a common preparation protocol. Figure 5 and Figure S7 show TEM images of cross-sectioned PC3 cells incubated with Au-CALNN-YIN NCs and Au-CALNN-INP NCs, respectively. After 30 min of incubation, AuNCs were found confined at the cellular membrane, suggesting the occurrence of ligand binding to the relevant NPY receptor. According to the TEM analyses, we speculated that mainly two internalization mechanisms were likely to take place, basically micropinocytosis and clathrin-mediated endocytosis. In most cases, a well-preserved double membrane of the vesicles characteristic of endocytosis pathway could be distinguished.

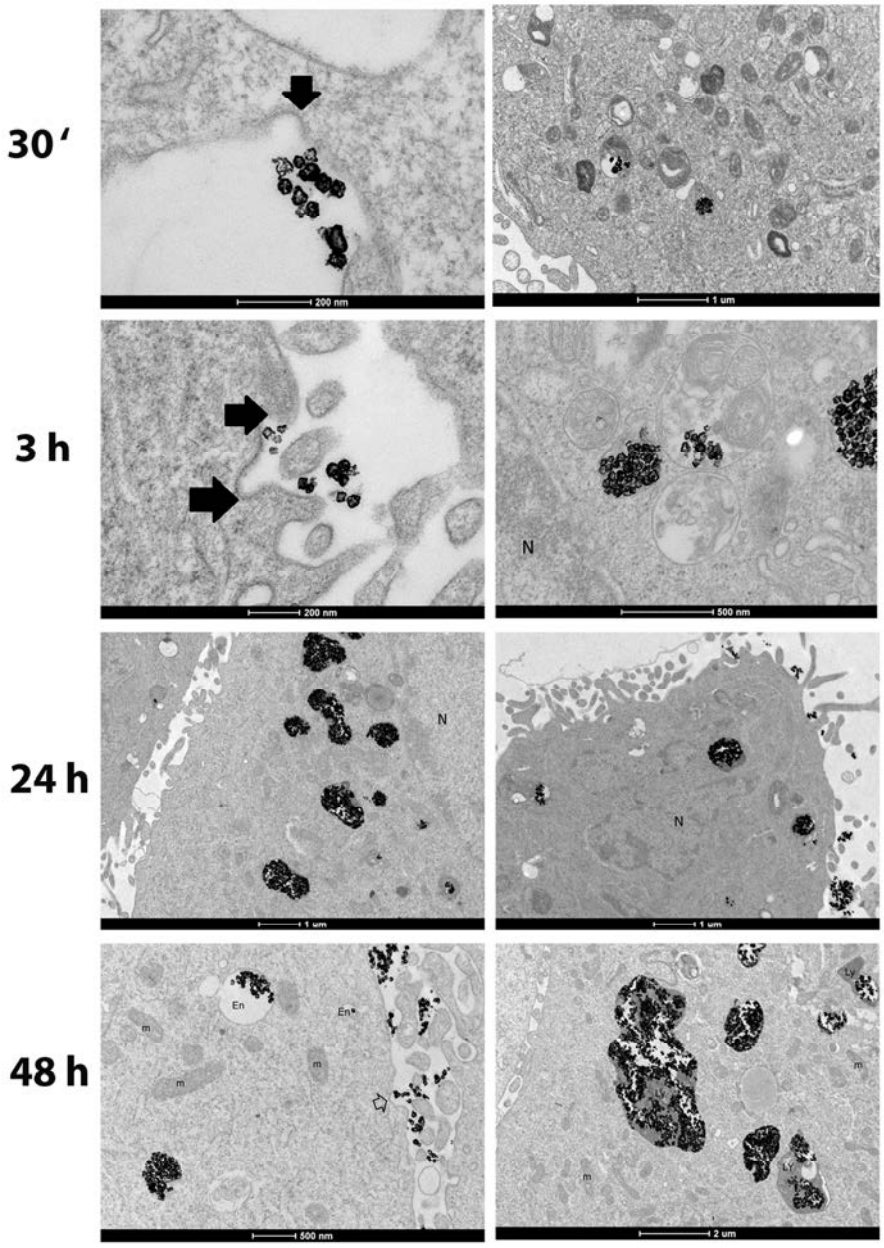

Figure 5. Gallery of TEM images showing cellular trafficking of Au-CALNN-YIN NCs in PC3 cells. The nanocages were incubated with cells for 30 min, 3, 5, 24 and 48 h, processed and visualized by TEM microscopy. Scale bars: a,c) 200 nm; b,e,f) 1 µm; d,g) 500 nm; h) 2 µm Small arrows indicate just internalized nanocages, while big arrows indicate clathrin formation.

Micropinocytosis took place here when aggregates of particles (i.e., > 300 nm) were interacting with the cell membrane, while clathrin-mediated endocytosis was favored in the case of a single particle-membrane interaction. A large extent of internalization of AuNCs by PC3 cells was evident already after short incubation time (3 h), while at longer incubation times (24 h and 48 h), the particles were found in the cytoplasm in huge amounts essentially confined into endosomes and/or lysosomes. In contrast to what has been reported with peptide-modified gold nanospheres, the presence of AuNCs free in cytoplasm was not detected under our experimental conditions. This could be interesting in view of a possible thermal effect. The presence of huge hot spots, compared to a generalized lower temperature increase that could be obtained by the internalization of individual nanocages free in the cytoplasm, could have also an effect on the fate of the cells after irradiation. Notably, Au-CALNN-INP NCs preferentially accumulated in endosomes, while Au-CALNN-YIN NCs were especially found inside lysosomes.

Although the cytosolic distribution of AuNCs was not expected to affect the outcome of laser treatments significantly, the accumulation of AuNCs in endosomes rather than in lysosomes could be instead of importance for the consequences it might have on the fate of the cell. In fact, the effect of laser treatment at different stages of nanoparticle confinement is currently under investigation in our laboratory. It is also curious to note the presence of nanoparticles close to the cellular membrane even after 48 h of incubation. This can be indicative of either exocytosis phenomena or prolonged cell uptake. As several images taken from different fields confirmed this observation, we reasoned that AuNCs could be partially exocytosed by the cells and subsequently re-endocytosed. A similar effect has been described in details by Kanaras et al. with spherical gold nanoparticles.[44] To confirm the hypothesis of the exocytosis/endocytosis mechanism, the cells were incubated with Au-CALNN-INP NCs and Au-CALNN-YIN NCs for

24 h, carefully washed with buffer to remove all residual nanocages from the matrix and re-incubated in the fresh media for additional 5 and 24 h. Figure 6 and Figure S8 show the presence of nanoparticles inside the vesicles throughout the cell, both close to the nucleus and to the cell membrane. As observed, vesicles were trafficked back to the cellular membrane and subsequently excreted. Eventually, exocytosed vesicles released the nanoparticles outside the cells, which were next endocytosed again (5 h and 24 h). The competitive action of faster and predominant endocytosis with slower relaxing exocytosis might be at the origin of the higher intracellular concentration of Au-CALLN-YIN constructs observed at 5 h (see Fig. 4 and Fig. S12) compared to the equilibrium value reached at longer incubation times (24 h).

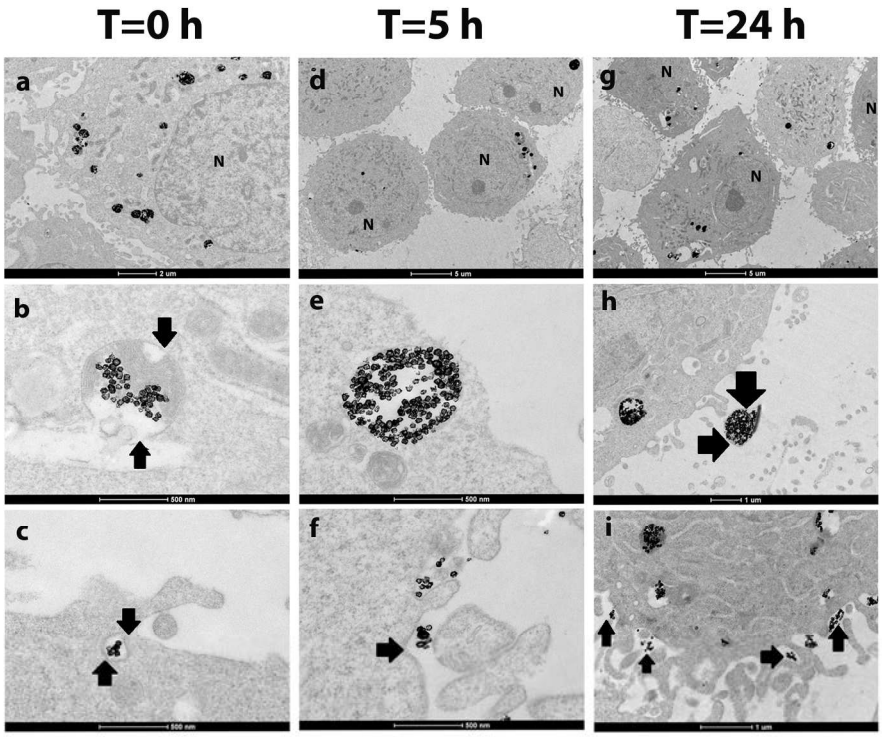

Figure 6. Gallery of TEM images showing PC3 cells incubated with Au-CALNN-YIN NCs: the cells were treated with nanocages for 24 h and washed with fresh medium (T = 0 h), then re-incubated for further 5 h (T = 5 h) or 24 h (T = 24 h). Scale bars: a) 2 μm; b,c,e,f) 500 nm; d,g) 5 μm; h,i) 1 μm.

Photothermal ablation of prostate cancer cells. Among different plasmonic nanoparticles, the interest in using gold nanocages as a tool for photothermal ablation of cancer has been dramatically rising thanks to their unique ability to absorb near-infrared (NIR) light in the 650−900 nm range, the so-called biologically transparent window.[45,46] Thus, we moved to investigate the efficiency of targeted AuNCs in inducing prostate cancer cell death via photothermal treatment. First, we studied the thermal-responsiveness of AuNCs in solution in order to define the maximum temperature rise at a given nanoparticle concentration (i.e., 0.4 nM). We exposed AuNCs in PBS to NIR laser irradiation at 800 nm with laser irradiance varying from 1.6 to 12.7 W/cm^2 for 20 min. Changes in temperature were measured and imaged by a thermographic camera over the whole duration of the experiments. As shown in Figure S9, the temperature of AuNCs increased from ca. 6 °C at the lowest irradiance (1.6 W/cm^2) to 35 °C at the highest (12.7 W/cm^2). In contrast, under the same conditions, the temperature of nanoparticle-free PBS solution increased only by 2 °C.

Next, to quantify the photothermal efficiency of nanoconjugates in cell cultures, we assessed the cell viability upon treatment with AuNCs. MTS assay was performed on PC3 cells incubated with nanoconjugates before and after laser irradiation. Cell viability was not compromised after incubation with peptide-conjugated AuNCs at 0.4 nM concentration for as long as 72 h of incubation (Figure S10). In contrast, upon irradiating the sample at an irradiance as low as 1.6 W/cm^2, cell viability drastically dropped even after the shortest irradiation time (30 sec) (Figure S11). At longer irradiation times, cell viability reached a plateau with similar values for all of the three nanoconjugates. Due to the experimental conditions, cell viability never reached zero values (a minimum 25% was found). This residual viability is likely attributable to the average fraction of cell pellet not irradiated In the Eppendorf tube due to the finite size of the laser spot

that should be confined in a small volume (1.6-1.8 mm linear size) in order to reach the desired irradiance value. Not surprisingly, cell viability was mostly compromised in the case of Au-CALNN-YIN NPs even after 30 s of irradiation. This result is in line with the cellular uptake studies showing the maximum accumulation of Au-CALNN-YIN NCs already after 3 h incubation, different from the other two nanoconjugates.

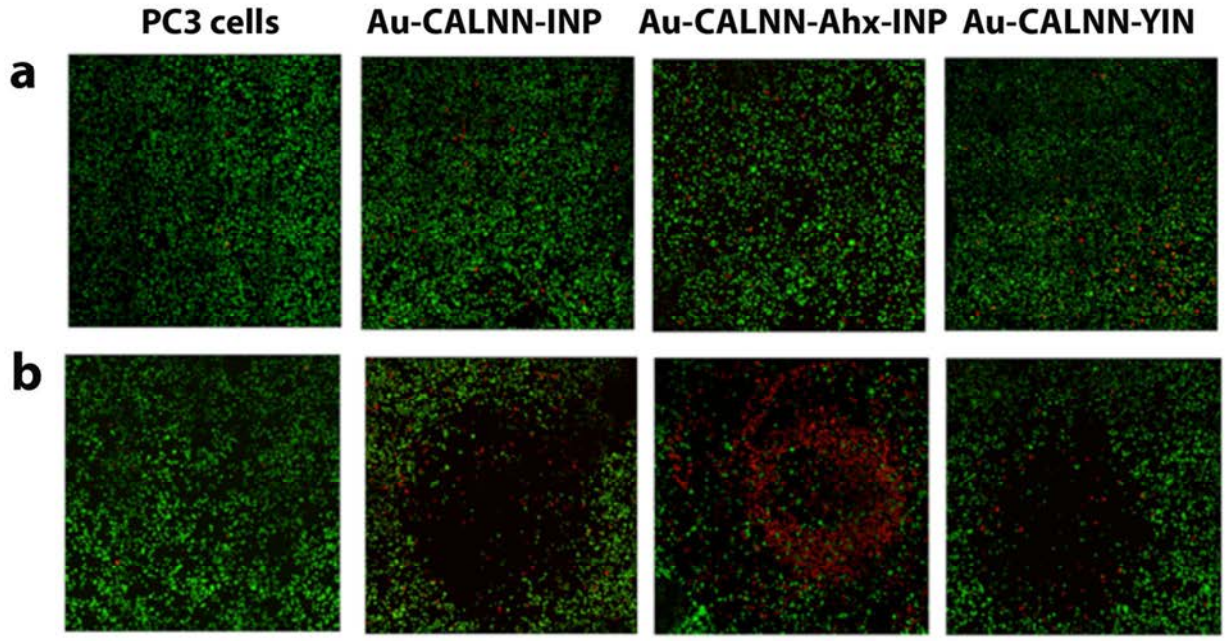

Figure 7. Fluorescence microscopy images of PC3 cells incubated with peptide-conjugated AuNCs: a) AuNCs upon NIR irradiation (800 nm, 12.7 W/cm^2) for 10 min; b) AuNCs upon NIR irradiation (800 nm, 12.7 W/cm^2) for 20 min. Viable cells are stained in green with calcein AM, dead cells are stained in red with PI. All images were collected in tile mode: the overall field of view is 3.1 · 3.1 mm.

In order to assess the tumorigenic cell ablation efficacy of peptide-conjugated AuNCs, we visualized the effect of NIR laser irradiation on a large field of view by means of confocal microscopy. All irradiation experiments were performed at room temperature. PC3 cells were cultured in a glass-bottomed Petri dish and incubated for 3 h with nanoconjugates at a final

concentration of 0.4 nM. Cells were irradiated for 10 and 20 min at 10 W/cm^2 irradiance, then stained with calcein AM and propidium iodide (PI) following a standard staining protocol and immediately observed by fluorescence microscopy. This assay is based on the conversion of the cell permeant non-fluorescent calcein AM dye to the fluorescent analog by intracellular esterase activity in live cells,[47] which allowed us to visualize the alteration of live/dead cells ratio caused by the photothermal effect of AuNCs. On the other hand, PI is membrane impermeable and does not enter viable cells with intact membranes, while once the cell undergoes membrane damage, PI intercalates into nucleic acids giving rise to dramatic fluorescence increase. As shown in Figure 7a, following 10 min of irradiation, the cells maintained their viability, even when treated with peptide-conjugated nanocages. When irradiation time was increased to 20 min, the cells underwent death principally by necrosis: a clear demarcation line between dead (red) and live (green) cell regions could be observed in the presence of AuNCs. By contrast, the irradiation of the untreated cells with the same laser power did not lead to cell death, confirming the safety of our experimental conditions. Moreover, the irradiation of plated cells at irradiance at 2 W/cm^2 or below did not produce any significant reduction of the calcein staining. This disagreement with the data from confocal microscopy raised a question: were the calcein-positive cells really alive or did they rather underwent cell death pathway, which could not be detected by this kind of staining? In order to resolve this question, more detailed studies on apoptosis pathway will be necessary. Temperature increase was recorded by a thermocamera while irradiating cells incubated either with Au-PVP NCs or with Au-peptide NCs. Thermograms shown in Figure 8 suggested that, at 12.7 W/cm^2 irradiance and 5 min irradiation time, control cells that were not incubated with AuNCs exhibited a negligible temperature change around 1 °C.

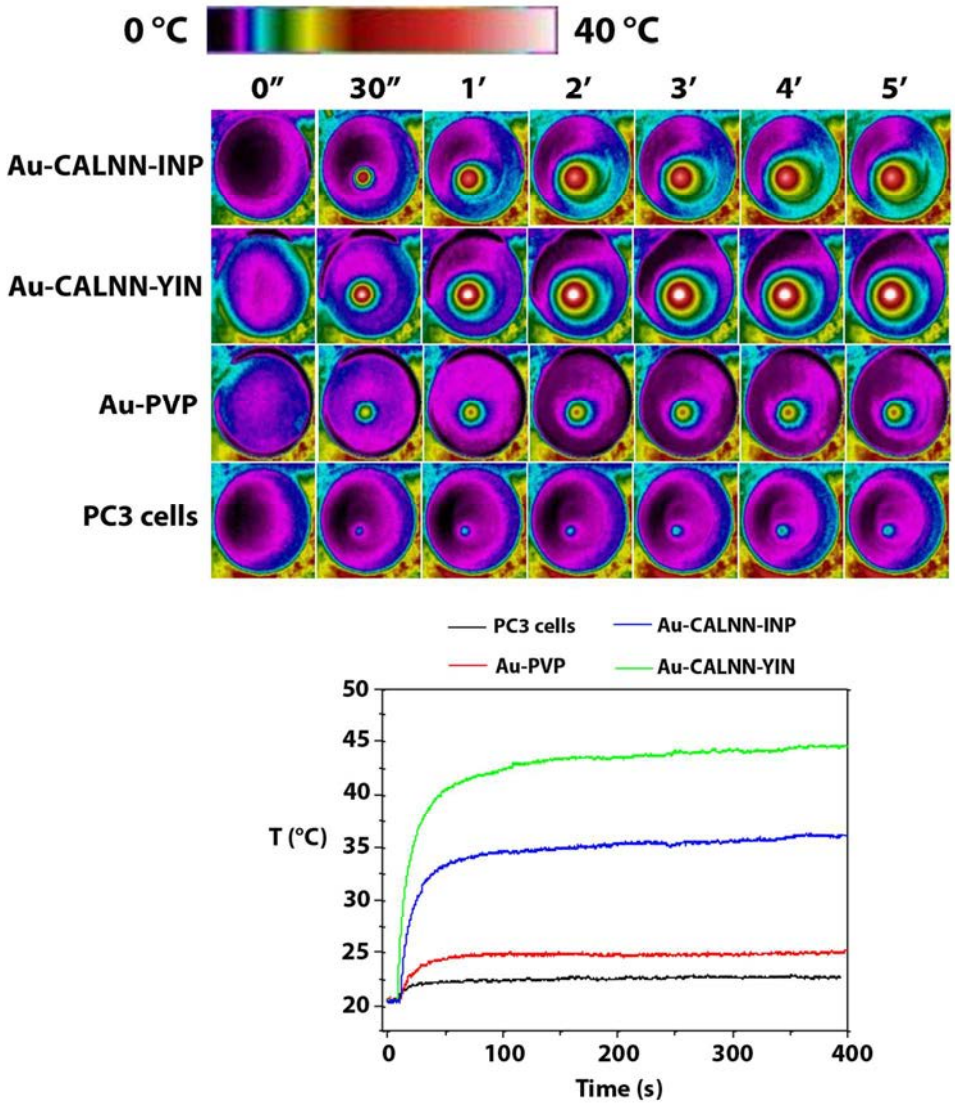

Figure 8. Upper panel: Time-dependent temperature-rise images of PC3 cells incubated with peptide-conjugated AuNCs, Au-PVP NCs and control cells. The pictures were obtained by thermocamera during laser exposure and show the Petri dish (35 mm diameter) with the central irradiated area. Lower panel: Time-dependent temperature-rise curves of PC3 cells incubated with peptide-conjugated AuNCs, Au-PVP NCs and control cells. Time interval: 5 min. Laser irradiance 12.7 W/cm^2, 800 nm.

When incubated with Au-PVP NCs, the temperature rise was slightly higher, but did not even reach 25 °C. This is in agreement with the low cellular uptake of these particles in PC3 cells. In contrast, when cells were incubated with Au-CALNN-INP NPs, the thermocamera revealed a significant heating with temperature approaching 35 °C, while even higher values, i.e., close to 44-45 °C, were reached with Au-CALNN-YIN NPs. These results are in accordance with MTS studies and fully correlate with cellular uptake assessment in PC3 cell cultures. Au-CALNN-YIN showed the major uptake and the lowest cell viability compared to the other samples. This temperature enhancement can be considered as an underestimated value of the actual temperature reached inside the cell, principally due to heat dissipation by the cell medium. However, our measurement could provide a good estimate of the heat pumped in the cell by the NIR absorption of the internalized nanocages, that leads to an intracellular temperature enhancement in the 10-20 degrees range.

Morphological changes of cell cytoskeleton upon laser treatment could give an idea of the occurred cellular damage. To perform these studies we used scanning electron microscopy (SEM). The cells, exposed to 10 min of laser irradiation at above conditions, were processed and analyzed by SEM. Temperature rise during irradiation experiment was monitored with thermocamera (Figure 8). The maximum temperature reached during irradiation was around 43 °C for Au-CALNN-YIN NCs, which correlates with the results of maximum cellular uptake. While the temperature of the cells, incubated with Au-PVP NCs did not show significant temperature rise, very similar to the control cells. Figure 9 indicates visible cellular damage after nanoparticle-induced hyperthermia. Untreated PC3 cells showed the presence of numerous characteristic microvilli on the cell surface both before and after exposure to NIR laser irradiation. In contrast, cells treated with Au-PVP NCs and exposed to NIR radiation showed

some morphological changes, such as membrane blebbing and partial reduction in microvilli exposure (Figure 9, c). Blebbing was indicative of occurred apoptosis after laser treatment when the cell becomes spherical, shaping itself as imposed by the cytoskeleton. As a next step, cell was digested and blebs or vesicles formed on its surface. On the other hand, cells treated with Au-PVP NCs but not exposed to the laser did not exhibit evidence of damage or apoptosis (Figure 9, d). PC3 cells showed complete loss of microvilli with simultaneous shrinkage in size compared to non-irradiated cells after treatment with Au-CALNN-INP NPs and exposed to NIR irradiation (Figure 9, e, f). Finally, cells treated with Au-CALNN-YIN NPs revealed a smoothening of cell surface showing complete loss of surface microvilli and a different morphological aspect compared to both Au-PVP NCs and Au-CALNN-INP NPs, suggesting a more relevant effect of hyperthermia on the cytoskeleton organization. The presence of microvilli on the surface of the malignant cells plays a role in cell migration, attachment and invasion, while reduction in microvilli may potentially inhibit cancer cell invasion and, therefore, prevent the disease development and diffusion.

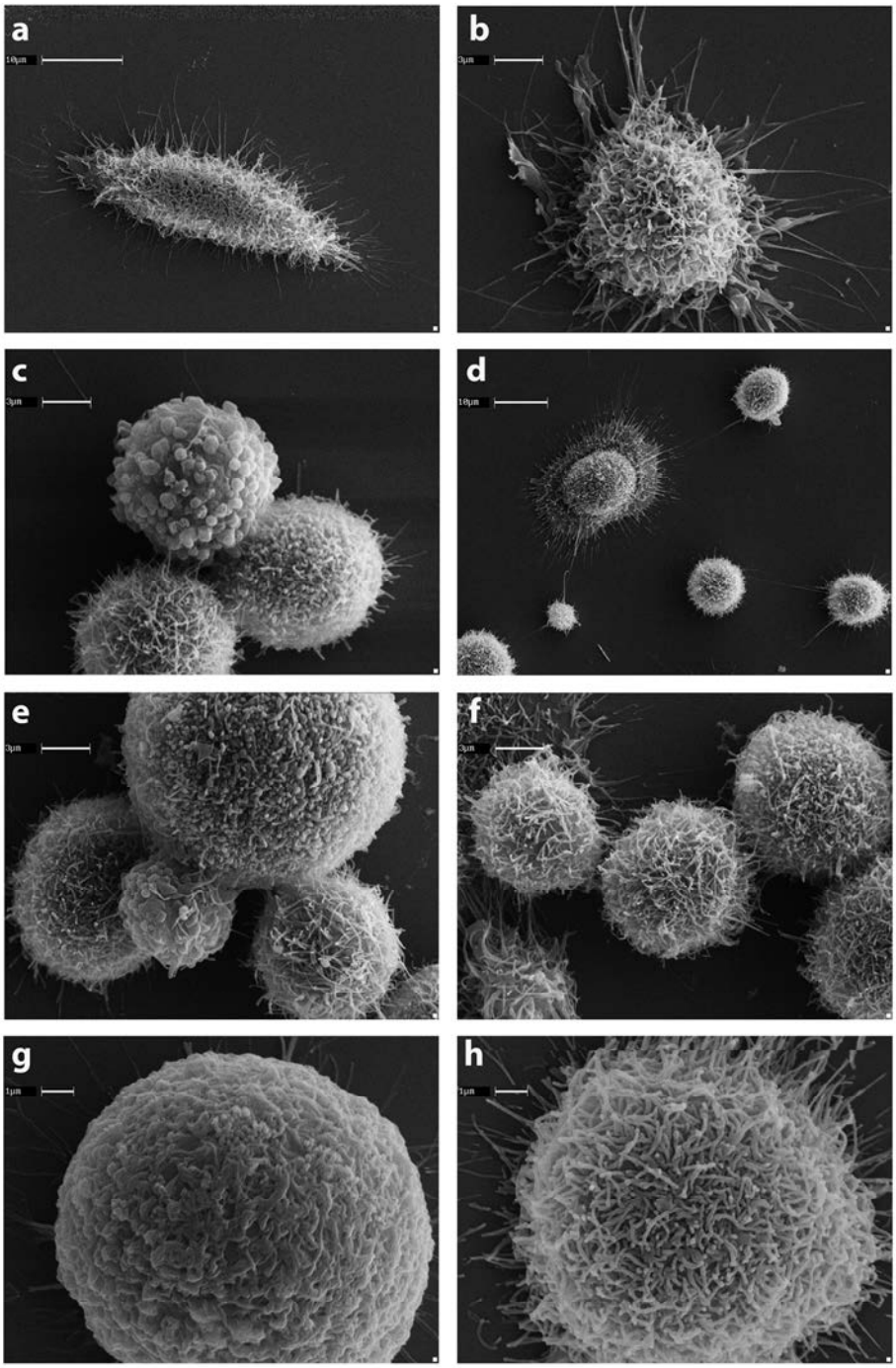

Figure 9. SEM images showing PC3 cell morphology changes pre- and post-hyperthermia treatment with AuNCs: a) untreated PC3 cells, b) PC3 cells irradiated with laser, c) PC3 cells incubated with Au-PVP NCs and irradiated with laser, d) PC3 cells incubated with Au-PVP NCs

without laser irradiation, e) PC3 cells incubated with Au-CALNN-INP NCs and irradiated with laser, f) PC3 cells incubated with Au-CALNN-INP NCs without laser irradiation, g) PC3 cells incubated with Au-CALNN-YIN NCs and irradiated with laser, and h) PC3 cells incubated with Au-CALNN-YIN NCs without laser irradiation. Scale bars: a,d) 10 μm; b,c,e,f) 3 μm; g,h) 1 μm.

CONCLUSIONS

In summary, the design, synthesis and characterization of monodisperse cubic-shaped gold nanocages functionalized with three different NPY analogs are reported in this study. The peptides were conjugated via a CALNN linker sequence and intercalated by short PEG molecules, allowing for an optimized self-assembly on the nanoparticle surface. The resulting Au-peptide NCs proved to be unexpectedly long-term stable in biological environment, as no cage degradation occurred even in 100% fetal bovine serum and in a broad range of pH (i.e., between 2 and 10). AuNCs were used to study the binding and internalization in a PC3 prostate cancer cell line, showing highly selective interaction with NPYR and efficient uptake promoted by clathrin-mediated endocytosis. TEM images showed a dynamic exchange of AuNCs between the cytosolic environment and the external cellular matrix, suggesting an active trafficking process of endocytosis/exocytosis/re-endocytosis across the cell membrane. Once loaded with AuNCs, cancer cells were irradiated with NIR laser at ca. 800 nm wavelength showing a heating enhancement dependent both on the irradiation intensity and nanoparticle uptake. Cells treated with Au-peptide NCs were irradiated at 10 W/cm^2 showing extensive necrosis after 20 min. However, further studies will be necessary to elucidate the possible involvement of apoptosis pathways in the mechanism of cell death. Interestingly, we observed significant morphological changes in the cell cytoskeleton caused by irradiation in PC3 cells bearing AuNCs, consistent with cellular damage. In particular, the appearance of membrane blebbing combined with loss of

characteristic microvilli could be associated to possible apoptosis and is expected to inhibit both proliferation and migration/invasion of cancer cells. The next steps of this research will be to go deeper into the elucidation of death mechanisms of cells loaded with NPY-AuNCs promoted by irradiation, and to investigate the intracellular pathways and protein expression activated or inhibited as a result of photothermal treatment. On the horizon of this study, we envisage numerous possible developments aimed at improving the diagnosis and treatment of different kinds of tumors well beyond prostate cancer, considering that neuropeptide receptor is found overexpressed in several malignancies, including glioblastoma, lymphomas, ovarian and breast carcinomas, neuroblastoma, small cell lung cancer, gastric and colorectal carcinomas.[48,49]

ASSOCIATED CONTENT

Supporting Information. Supporting Information is available free of charge on the ACS Publications website. Peptide sequences, chemical structure and purity, peptide synthesis, AuNCs preparation and functionalization, experimental methods, and supporting figures S1-S11 (all included in one pdf file).

AUTHOR INFORMATION

Corresponding Author

* Davide Prosperi: davide.prosperi@unimib.it

Author Contributions

The manuscript was written through contributions of all authors. All authors have given approval to the final version of the manuscript.

Notes

The authors declare no competing financial interest.

ACKNOWLEDGMENT

S.A. acknowledges European Soft Matter Infrastructure (ESMI) program, Prof. Luis Liz-Marzàn and Ana Sanchez-Iglesias at biomaGUNE, San Sebastiàn, Spain. We especially thank Raffaele Allevi (University of Milano) for help with electron microscopy and Stefania Brambilla for the execution of mass spectrometry analyses. This project was supported by the Fondazione Regionale per la Ricerca Biomedica of Regione Lombardia (FRRB to D.P. and M.C.) and by Academic Funding Unimib 2014 to M.C and L.S.

REFERENCES

(1) Weiner, G. J. (2015) Building Better Monoclonal Antibody-Based Therapeutics. Nat. Rev. Cancer, 15, 361–370.

(2) Wurz, G. T.; Kao, C. J.; De Gregorio, M. W. (2016) Novel Cancer Antigens for Personalized Immunotherapies: Latest Evidence and Clinical Potential. Ther. Adv. Med. Oncol. 8, 4–31.

(3) Chames, P.; Van Regenmortel, M.; Weiss, E.; Baty, D. (2009) Therapeutic Antibodies: Successes, Limitations and Hopes for the Future. Br. J. Pharmacol., 157, 220–233.

(4) Shefet-Carasso, L.; Benhar, I. (2015) Antibody-Targeted Drugs and Drug Resistance – Challenges and Solutions. Drug Resist. Updates, 18, 36–46.

(5) Morgat, C.; Mishra, A. K.; Varshney, R.; Allard, M.; Fernandez, P.; Hindié, E. (2014) Targeting Neuropeptide Receptors for Cancer Imaging and Therapy: Perspectives with Bombesin, Neurotensin, and Neuropeptide-Y Receptors. J. Nucl. Med., 55, 1650–1657.

(6) Reubi, J.C. (2003) Peptide Receptors as Molecular Targets for Cancer Diagnosis and Therapy. Endocrine Rev., 24, 389–427.

(7) Jensen, R. T. (2000) Carcinoid and Pancreatic Endocrine Tumors: Recent Advances in Molecular Pathogenesis, Localization, and Treatment. Curr. Opin. Oncol., 12, 368–377.

(8) Fani, M.; Maecke, H. R.; Okarvi, S. M. (2012) Radiolabeled Peptides: Valuable Tools for the Detection and Treatment of Cancer. Theranostics, 2, 481–501.

(9) Huanga, H.-C.; Baruaa, S.; Sharmad, G.; Deyb, S. K.; Rege, K. (2011) Inorganic Nanoparticles for Cancer Imaging and Therapy. J. Controlled Rel., 155, 344–357.

(10) Xia, Y.; Li, W.; Cobley, C. M.; Chen, J.; Xia, X.; Zhang, Q.; Yang, M.; Cho, E. C.; Brown, P. K. (2011) Gold Nanocages: from Synthesis to Theranostic Applications. Acc. Chem. Res., 44, 914–924.

(11) Eichelbaum, M.; Schmidt, B.E.;Ibrahim, H., Rademann, K. (2007) Three-Photon-Induced Luminescence of Gold Nanoparticles Embedded in and Located on the Surface of Glassy Nanolayers Nanotechnology, 18, 355702.

(12) Meir, R.; Motiei, M.; Popovtzer, R. (2014) Gold Nanoparticles for In Vivo Cell Tracking. Nanomedicine, 9, 2059–2069.

(13) Zhang, Q.; Iwakuma, N.; Sharma, P.; Moudgil, B.M.; Wu, C.; McNeill, J.; Jiang, H.; Grobmyer, S.R. (2009) Gold Nanoparticles as a Contrast Agent for In Vivo Tumor Imaging with Photoacoustic Tomography. Nanotechnology, 20, 395102.

(14) Shi, P.; Liu, Z.; Dong, K.; Ju, E.; Ren, J.; Du, Y.; Li, Z.; Qu, X. (2014) A Smart "Sense-Act-Treat" System: Combining a Ratiometric pH Sensor with a Near Infrared Therapeutic Gold Nanocage. Adv Mater., 26, 6635-6641.

(15) Shi, P.; Li, M.; Ren, J.; Qu, X. (2013) Gold Nanocage-Based Dual Responsive "Caged Metal Chelator" Release System: Noninvasive Remote Control with Near Infrared for Potential Treatment of Alzheimer's Disease. Advanced Functional Materials, 23, 5412-5419.

(16) Moran, C. H.; Wainerdi, S. M.; Cherukuri, T. K.; Kittrell, C.; Wiley, B. J.; Nicholas, N. W.; Curley, S. A.; Kanzius, J. S.; Cherukuri. P. (2009) Size-Dependent Joule Heating of Gold Nanoparticles Using Capacitively Coupled Radiofrequency Fields. Nano Res., 2, 400–405.

(17) Cardinal, J.; Klune. J. R.; Chory, E.; Jeyabalan, G.; Kanzius, J. S.; Nalesnik, M.; Geller, D. A. (2008) Noninvasive Radiofrequency Ablation of Cancer Targeted by Gold Nanoparticles. Surgery, 144, 125–132.

(18) Chen, F.; Cai, W. (2015) Nanomedicine for Targeted Photothermal Cancer Therapy: Where Are We Now? Nanomedicine, 10, 1–3.

(19) Hwang, S.; Nam, J.; Jung, S.; Song, J.; Doh, H.; Kim, S. (2014) Gold Nanoparticle-Mediated Photothermal Therapy: Current Status and Future Perspective. Nanomedicine, 9, 2003–2022.

(20) Rozengurt, E. (2002) Neuropeptides as Growth Factors for Normal and Cancerous Cells. Trends Endocrinol. Metab., 13, 128–134.

(21) Ruscica, M.; Dozio, E.; Boghossian, S.; Bovo, G.; Martos Riaño, V.; Motta, M.; Magni, P. (2006) Activation of the Y1 Receptor by Neuropeptide Y Regulates the Growth of Prostate Cancer Cells. Endocrinology, 147, 1466–1473.

(22) Cabrele C., Beck-Sickinger A. G. (2000) Molecular Characterization of the Ligand–Receptor Interaction of the Neuropeptide Y Family. J. Peptide Sci., 6, 97–122.

(23) Lévy, R.; Thanh, N. T. K.; Doty, C. R.; Hussain, I.; Nichols, R. J.; Schiffrin, D. J.; Brust, M.; Fernig, D. G. (2004) Rational and Combinatorial Design of Peptide Capping Ligands for Gold Nanoparticles. J. Am. Chem. Soc., 126, 10076–10084.

(24) Allen, J.; Novotný, J.; Martin, J.; Heinrich, G. (1987) Molecular Structure of Mammalian Neuropeptide Y: Analysis by Molecular Cloning and Computer-Aided Comparison with Crystal Structure of Avian Homologue. Proc. Natl. Acad. Sci. USA, 84, 2532–2536.

(25) Leban J. J.; Heyer D.; Landavazo A.; Matthews J.; Aulabaugh A.; Daniels A. J. (1995) Novel Modified Carboxy Terminal Fragments of Neuropeptide Y with High Affinity for Y2-Type Receptors and Potent Functional Antagonism at a Y1-Type Receptor. J. Med. Chem., 38, 1150–1157.

(26) Whitmore, L.; Wallace, B. A. (2008) Protein Secondary Structure Analyses from Circular Dichroism Spectroscopy: Methods and Reference Databases. Biopolymers, 89, 392–400.

(27) Andrade, M. A.; Chacón, P.; Merelo, J. J.; Morán, F. (1993) Evaluation of Secondary Structure of Proteins from UV Circular Dichroism Spectra Using an Unsupervised Learning Neural Network. Prot. Engineering, 6, 383–390.

(28) Zhang, Q.; Li, W.; Wen, L. P.; Chen, J.; Xia, Y. (2010) Facile Synthesis of Ag Nanocubes of 30 to 70 nm in Edge Length with CF_3COOAg as a Precursor. Chem. Eur. J., 16, 10234–10239.

(29) Khlebtsov, B. et al. (2011) Nanocomposites Containing Silica-Coated Gold–Silver Nanocages and Yb–2,4-Dimethoxyhematoporphyrin: Multifunctional Capability of IR-Luminescence Detection, Photosensitization, and Photothermolysis. ACS Nano, 5, 7077–7089.

(30) Lévy, R. (2006) Peptide-Capped Gold Nanoparticles: Towards Artificial Proteins. ChemBioChem, 7, 1141–1145.

(31) Blanco, E.; Shen, H.; Ferrari, M. (2015) Principles of Nanoparticle Design for Overcoming Biological Barriers to Drug Delivery. Nat. Biotechnol., 33, 941–951.

(32) Heikkilä, E.; Martinez-Seara, H.; Gurtovenko, A. A.; Javanainen, M.; Hakkinen, H.; Vattulainen, I.; Akola, J. (2014) Cationic Au Nanoparticle Binding with Plasma Membrane-like Lipid Bilayers: Potential Mechanism for Spontaneous Permeation to Cells Revealed by Atomistic Simulations. J. Phys. Chem. C, 118, 11131–11141.

(33) Lin, J.; Alexander-Katz, A. (2013) Cell Membranes Open “Doors” for Cationic Nanoparticles/Biomolecules: Insights into Uptake Kinetics. ACS Nano, 7, 10799–10808.

(34) Fiandra, L.; Mazzucchelli, S.; De Palma, C.; Colombo, M.; Allevi, R.; Sommaruga, S.; Clementi, E.; Bellini, M.; Prosperi, D.; Corsi, F. (2013) Assessing the In Vivo Targeting

Efficiency of Multifunctional Nanoconstructs Bearing Antibody-Derived Ligands. ACS Nano, 7, 6092–6102.

(35) Avvakumova, S.; Fezzardi, P.; Pandolfi, L.; Colombo, M.; Sansone, F.; Casnati, A.; Prosperi, D. (2014) Gold Nanoparticles Decorated by Clustered Multivalent Cone-Glycocalixarenes Actively Improve the Targeting Efficiency Toward Cancer Cells. Chem. Commun., 50, 11029–11032.

(36) Avvakumova, S.; Galbiati, E.; Pandolfi, L.; Mazzucchelli, S.; Cassani, M.; Gori, A.; Longhi, R.; Prosperi, D. (2014) Development of U11-Functionalized Gold Nanoparticles for Selective Targeting of Urokinase Plasminogen Activator Receptor-Positive Breast Cancer Cells. Bioconjugate Chem., 25, 1381–1386.

(37) Zhang, W.; Liu, H. T. (2002) MAPK Signal Pathways in the Regulation of Cell Proliferation in Mammalian Cells. Cell Res., 12, 9–18; b) McCubrey; J. A.; Steelman, L. S.; Chappell, W. H., Abrams, S. L.

(38) Wong, E. W. T. et al. (2007) Roles of the Raf/MEK/ERK Pathway in Cell Growth, Malignant Transformation and Drug Resistance. Biochim. Biophys. Acta, 1773, 1263–1284.

(39) Chang, F.; Steelman, L. S.; Lee, J. T.; Shelton, J. G.; Navolanic, P. M.; Blalock, Wl L.; Franklin, R. A.; McCubrey, J. A. (2003) Signal Transduction Mediated by the Ras/Raf/MEK/ERK Pathway from Cytokine Receptors to Transcription Factors: Potential Targeting for Therapeutic Intervention. Leukemia, 17, 1263–1293.

(40) Kilinc, D.; Lesniak, A.; Rashdan, S. A.; Gandhi, D.; Blasiak, A.; Fannin, P. C.; von Kriegsheim, A.; Kolch, W.; Lee, G. U. (2015) Mechanochemical Stimulation of MCF7 Cells

with Rod-Shaped Fe–Au Janus Particles Induces Cell Death Through Paradoxical Hyperactivation of ERK. Adv. Healthcare. Mat., 4, 395–404.

(41) Jiang, W.; Kim, B. Y. S.; Rutka, J. T.; Chan, W. C. W. (2008) Nanoparticle-Mediated Cellular Response Is Size-Dependent. Nat. Nanotech., 3, 145–150.

(42) Kim, C. S.; Li, X.; Jiang, Y.; Yan, B.; Tonga, G. Y.; Ray, M.; Solfiell, D. J.; Rotello , V. M. (2015) Cellular Imaging of Endosome Entrapped Small Gold Nanoparticles. Methods, 2, 306–315.

(43) Bouzin, M.; Sironi, L.; Chirico, G.; D'Alfonso, L.; Inverso, D.; Pallavicini, P. Collini, M. (2015) An Intermittent Model for Intracellular Motions of Gold Nanostars by k-Space Scattering Image Correlation. Biophys. J., 109, 2246–2258.

(44) Grundemar, L., Ed.; Bloom, S. R. (1997) Ed. Neuropeptide Y and Drug Development; Academic Press.

(45) Bartczak, D.; Nitti, S.; Millar, T. M.; Kanaras, A. G. (2012) Exocytosis of Peptide Functionalized Gold Nanoparticles in Endothelial Cells. Nanoscale, 4, 4470–4472.

(46) Pansare, V.; Hejazi, S.; Faenza, W.; Prud'homme, R. K. (2012) Review of Long-Wavelength Optical and NIR Imaging Materials: Contrast Agents, Fluorophores, and Multifunctional Nano Carriers. Chem. Mater., 24, 812–827.

(47) Wang, Z.; Chen, Z.; Liu, Z.; Shi, P.; Dong, K.; Ju, E.; Ren, J.; Qu, X. (2014) A Multi-Stimuli Responsive Gold Nanocage-Hyaluronic Platform for Targeted Photothermal and Chemotherapy. Biomaterials, 35, 9678–9688.

(48) Piao J.-G.; Liu, D.; Hu, K.; Wang, L.; Gao, F.; Xiong, Y.; Yang, L. (2016) Cooperative Nanoparticle System for Photothermal Tumor Treatment without Skin Damage. ACS Appl. Mater. Interfaces, 8, 2847–2856.

(49) Li, J.; Tian, Y.; Wu, A. (2015) Neuropeptide Y Receptors: A Promising Target for Cancer Imaging and Therapy. Regener. Biomater. 2, 215–219.

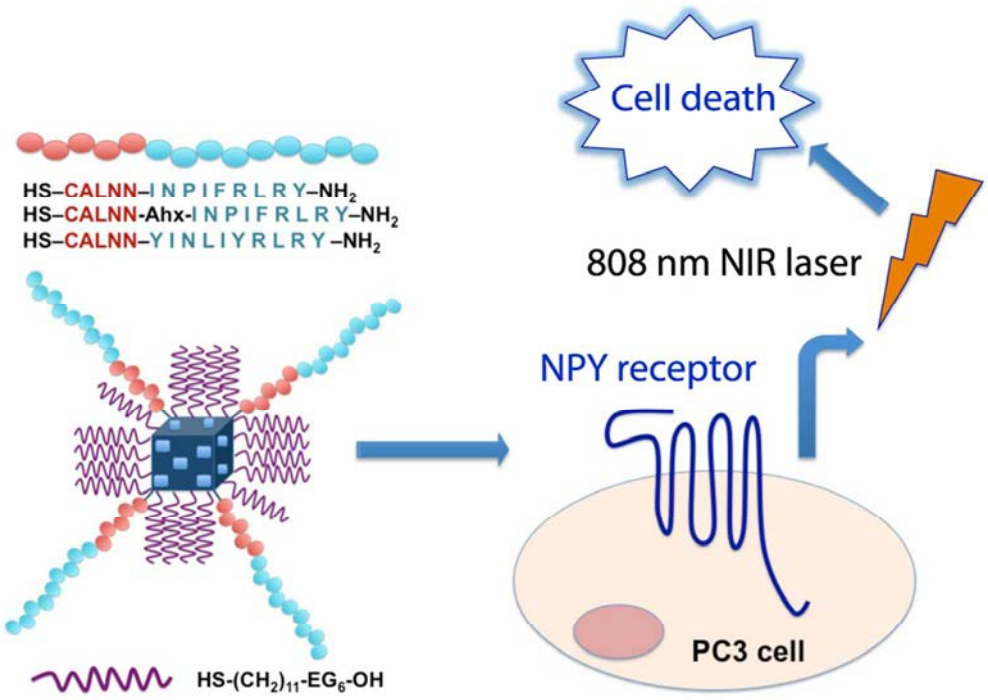

Figure 1. Schematic representation of NPYR targeting on prostate cancer cells by peptide-functionalized gold nanocages and subsequent hyperthermia by NIR irradiation. Three kinds of AuNCs are considered, deriving from the surface functionalization with selected peptides, namely a) CALNN-INP, b) Au-CALNN-Ahx-INP, c) Au-CALNN-YIN, respectively. Peptide sequences are sketched in the figure. The available surface of AuNCs was saturated by short PEG molecules, HS-(CH2)11-EG6-OH.

80x59mm (300 x 300 DPI)

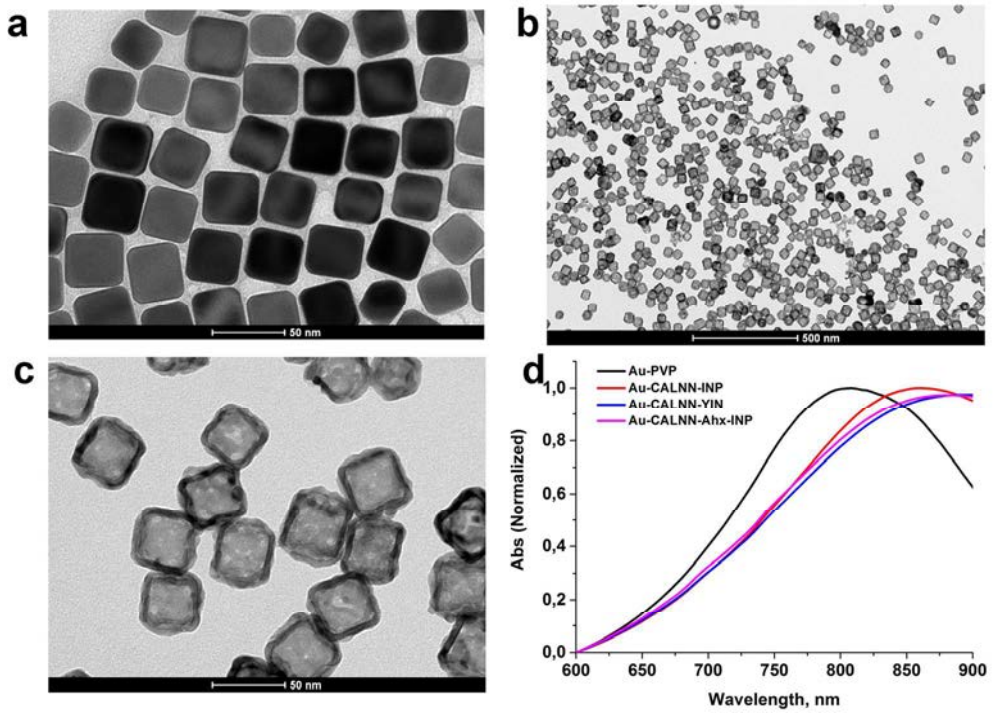

Figure 2. a) TEM micrographs of as-prepared silver nanocubes - medium size 34.7 ± 2.5 nm (scale bar 50 nm); b) TEM micrographs of as-prepared Au-PVP NCs (scale bar 500 nm); c) TEM micrographs of as-prepared Au-PVP NCs – medium size 40.8 ± 1.8 nm (scale bar 50 nm); d) UV-vis spectra of AuNCs before and after functionalization with peptides.

140x99mm (300 x 300 DPI)

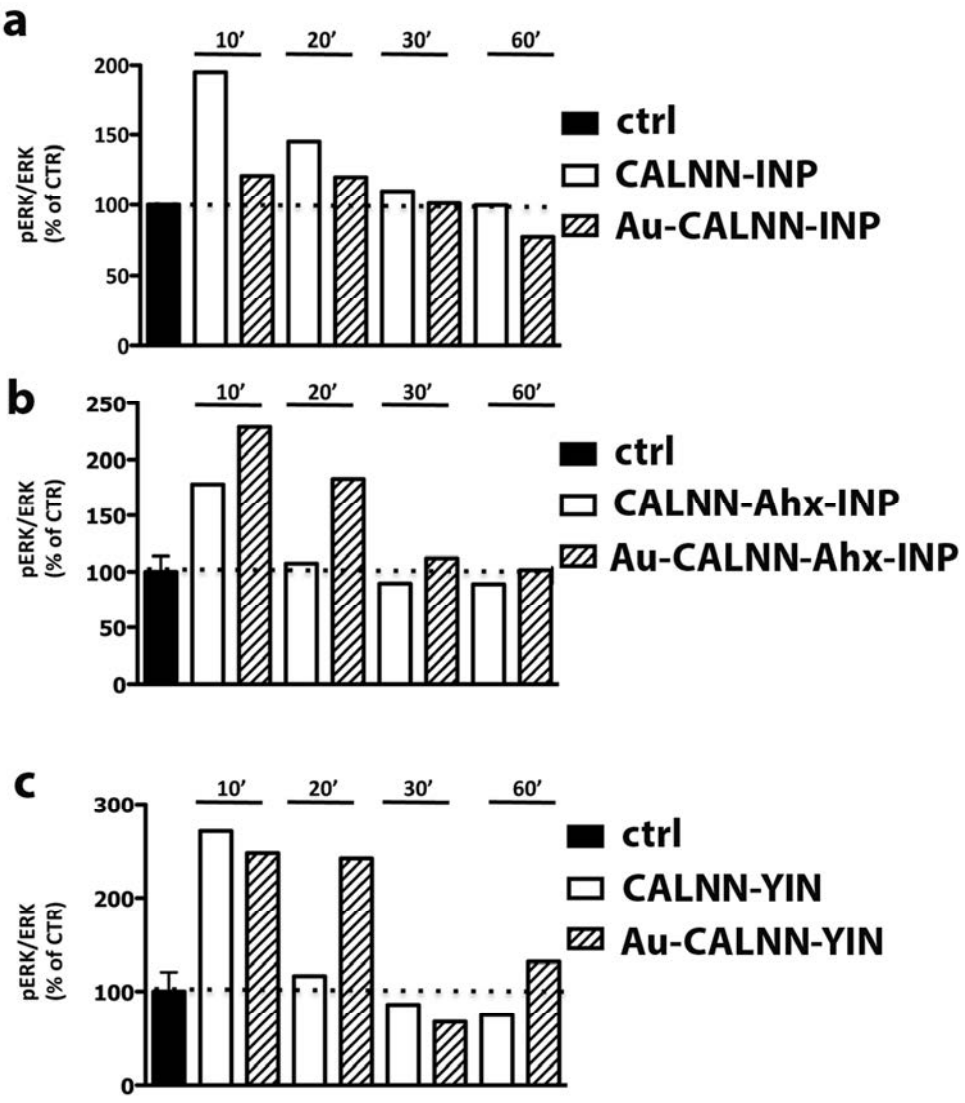

Figure 3. Time dependence of ERK phosphorylation in PC3 cells in response to specific NPYR targeting by nanocages decorated with a) CALNN-INP, b) CALNN-Ahx-INP, and c) CALNN-YIN peptides. Number of replicates, n = 3.

139x156mm (200 x 200 DPI)

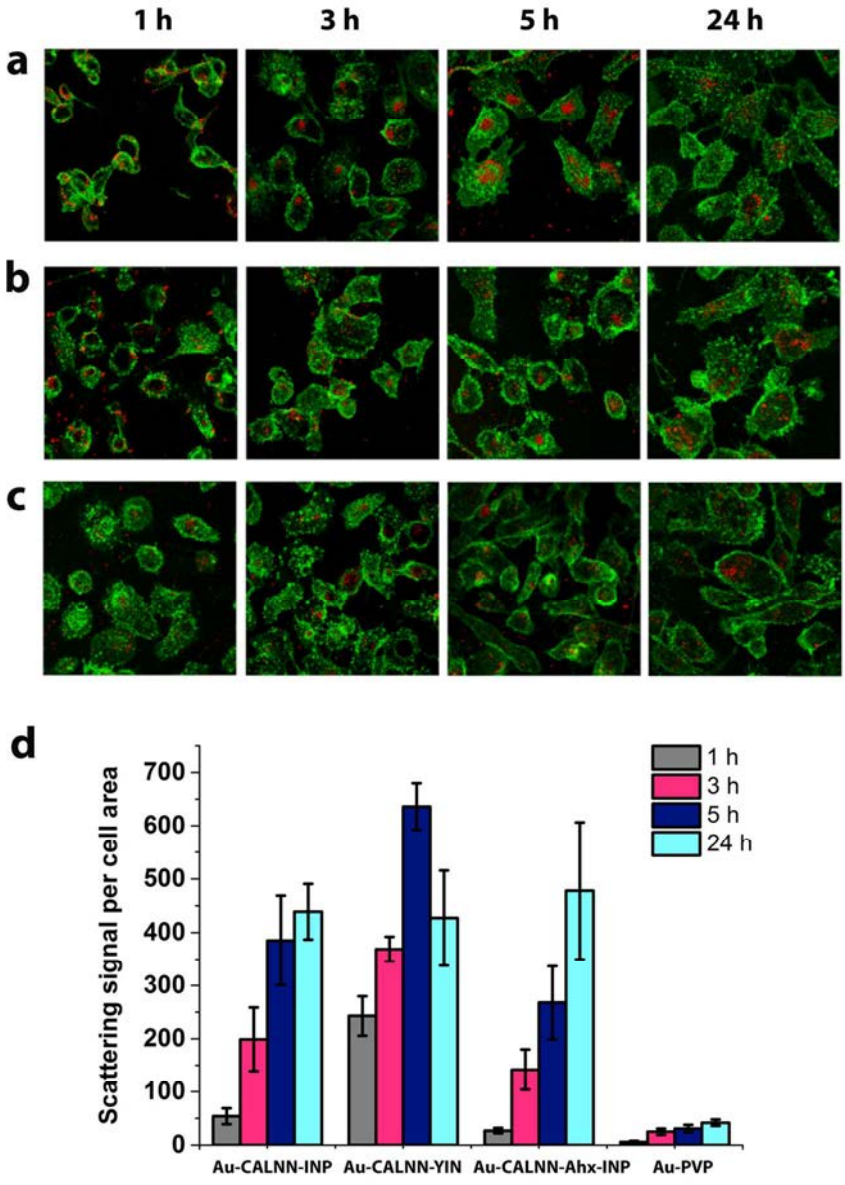

Figure 4. Confocal microscopy images (162 μm × 162 μm) of PC3 cells incubated with peptide-functionalized AuNCs: a) Au-CALNN-INP NPs; b) Au-CALNN-Ahx-INP NPs; c) Au-CALNN-YIN NPs. Cellular membranes are stained with AlexaFluor488–conjugated Wheat germ agglutinin (green), while AuNCs are visualized in reflection mode (red); d) Cellular uptake quantification by confocal microscopy. Scattering signal per cell area is reported after measuring at least 50 cells per sample. The nanoparticle uptake, evaluated by summing the scattering signal from all the nanoparticles inside each cell normalized to the cell section area, was averaged over at least 50 cells.

107x150mm (300 x 300 DPI)

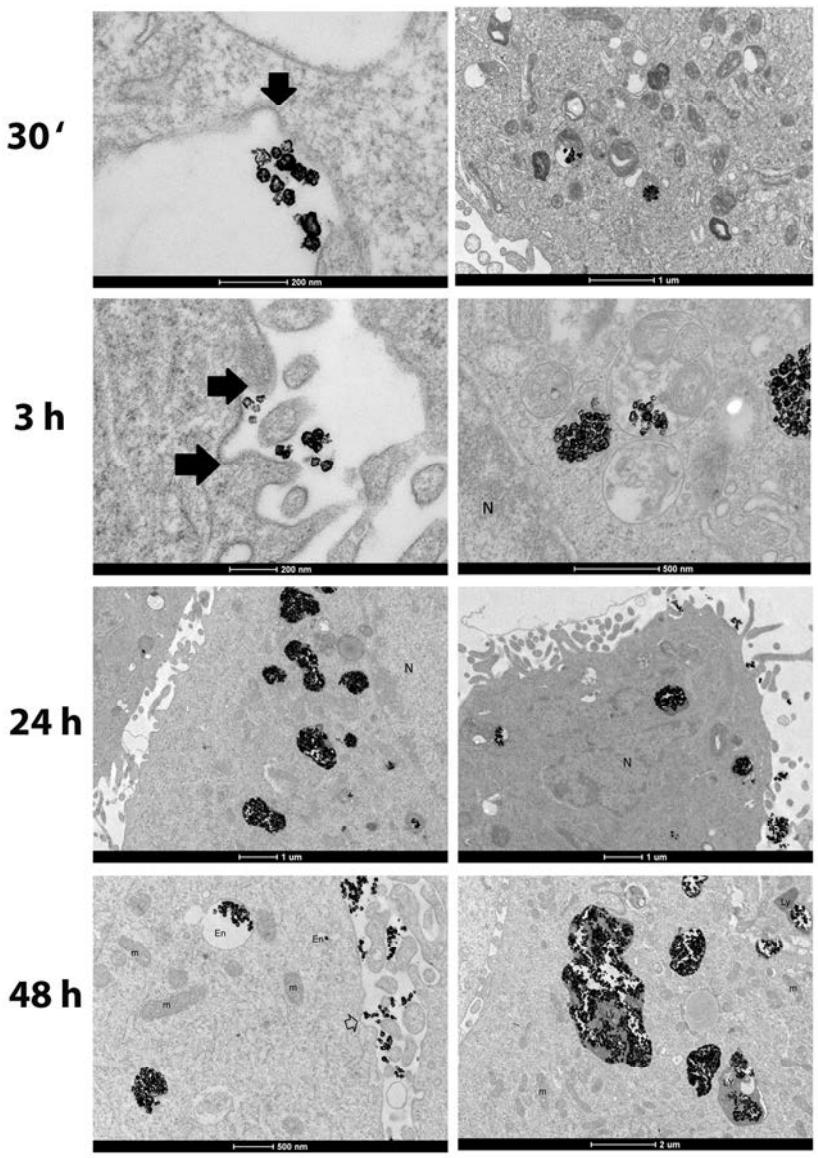

Figure 5. Gallery of TEM images showing cellular trafficking of Au-CALNN-YIN NCs in PC3 cells. The nanocages were incubated with cells for 30 min, 3, 5, 24 and 48 h, processed and visualized by TEM microscopy. Scale bars: a,c) 200 nm; b,e,f) 1 μm; d,g) 500 nm; h) 2 μm Small arrows indicate just internalized nanocages, while big arrows indicate clathrin formation.

119x171mm (300 x 300 DPI)

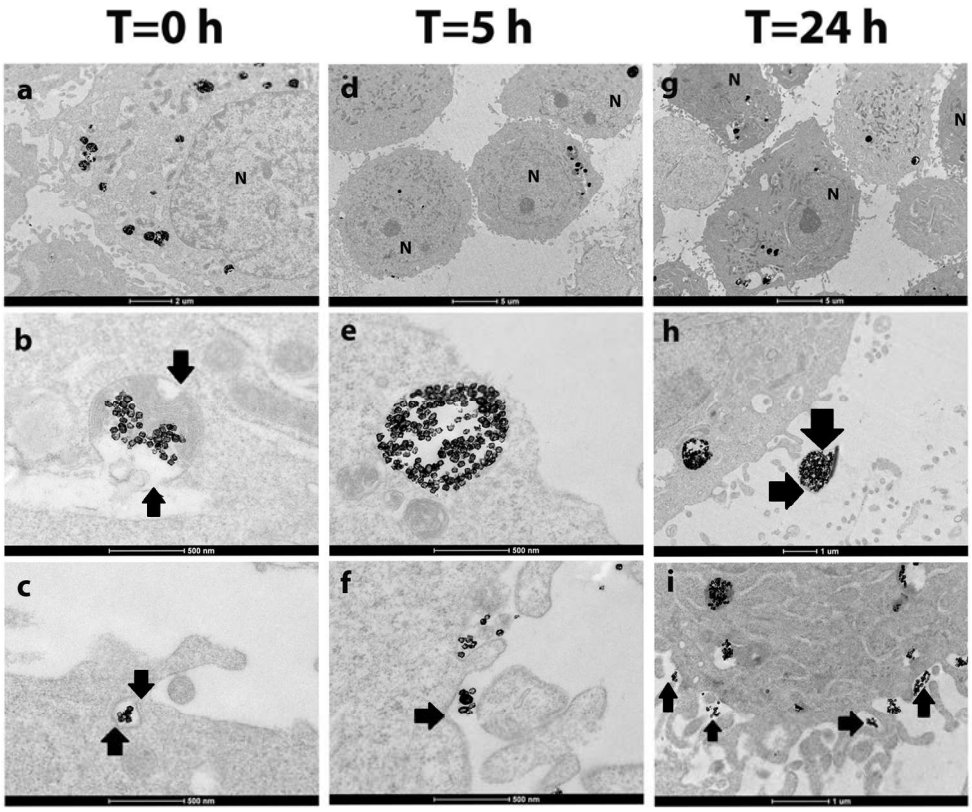

Figure 6. Gallery of TEM images showing PC3 cells incubated with Au-CALNN-YIN NCs: the cells were treated with nanocages for 24 h and washed with fresh medium (T = 0 h), then re-incubated for further 5 h (T = 5 h) or 24 h (T = 24 h). Scale bars: a) 2 µm; b,c,e,f) 500 nm; d,g) 5 µm; h,i) 1 µm.

177x148mm (300 x 300 DPI)

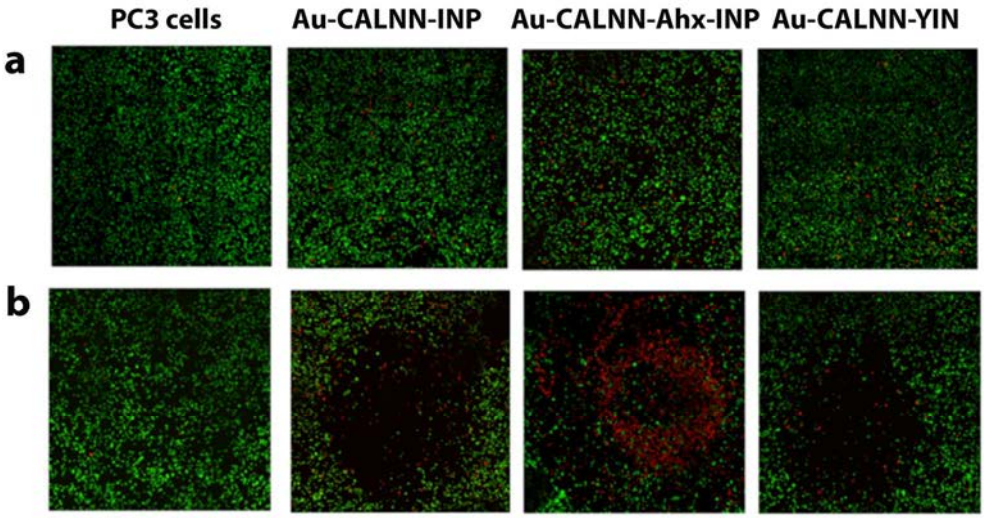

Figure 7. Fluorescence microscopy images of PC3 cells incubated with peptide-conjugated AuNCs: a) AuNCs upon NIR irradiation (800 nm, 12.7 W/cm2) for 10 min; b) AuNCs upon NIR irradiation (800 nm, 12.7 W/cm2) for 20 min. Viable cells are stained in green with calcein AM, dead cells are stained in red with PI. All images were collected in tile mode: the overall field of view is 3.1 × 3.1 mm.

119x64mm (300 x 300 DPI)

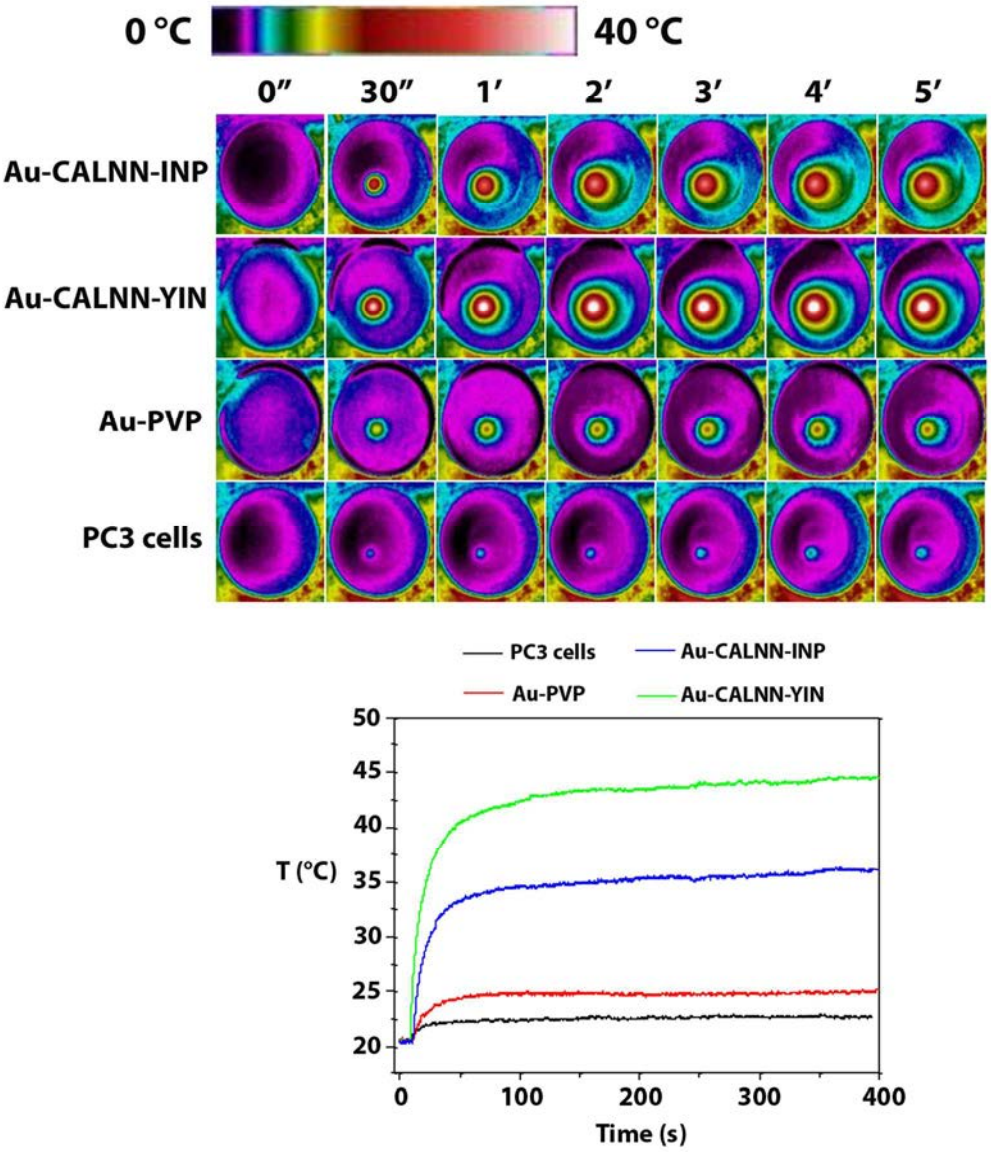

Figure 8. Upper panel: Time-dependent temperature-rise images of PC3 cells incubated with peptide-conjugated AuNCs, Au-PVP NCs and control cells. The pictures were obtained by thermocamera during laser exposure and show the Petri dish (35 mm diameter) with the central irradiated area. Lower panel: Time-dependent temperature-rise curves of PC3 cells incubated with peptide-conjugated AuNCs, Au-PVP NCs and control cells. Time interval: 5 min. Laser irradiance 12.7 W/cm^2, 800 nm.

160x188mm (200 x 200 DPI)

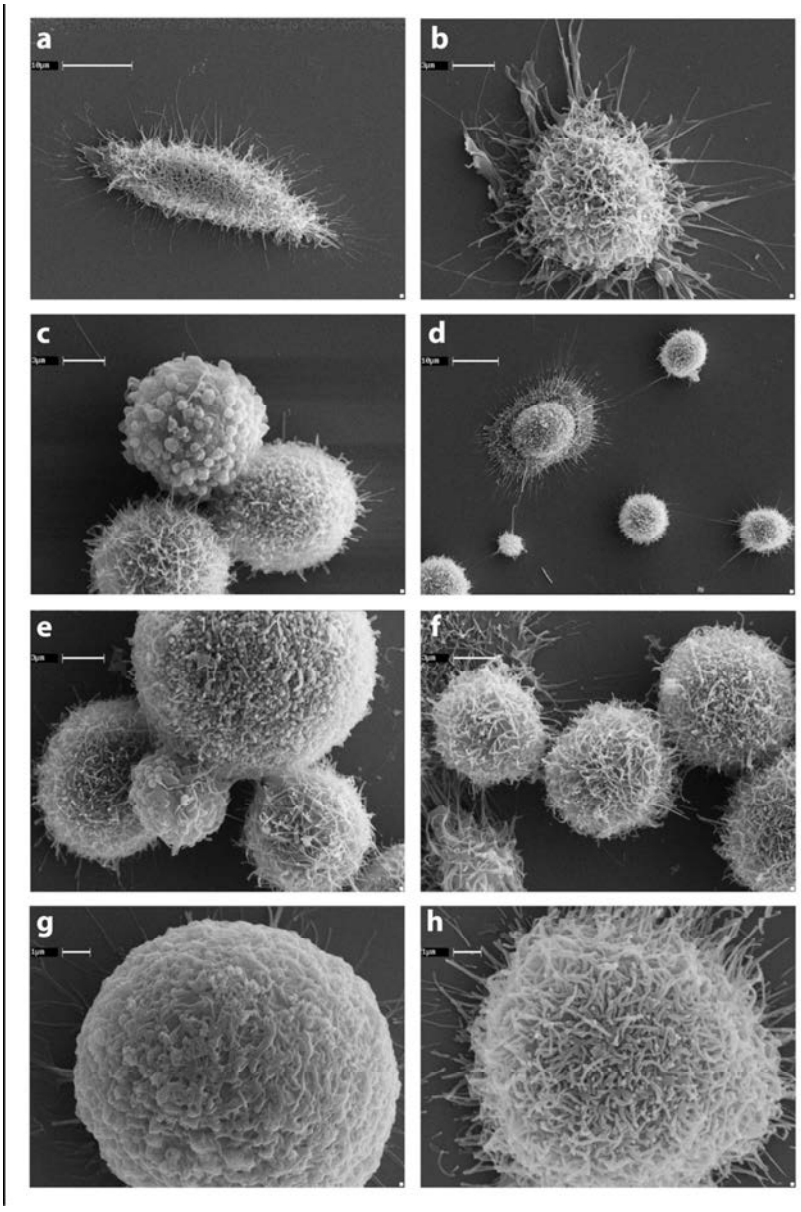

Figure 9. SEM images showing PC3 cell morphology changes pre- and post-hyperthermia treatment with AuNCs: a) untreated PC3 cells, b) PC3 cells irradiated with laser, c) PC3 cells incubated with Au-PVP NCs and irradiated with laser, d) PC3 cells incubated with Au-PVP NCs without laser irradiation, e) PC3 cells incubated with Au-CALNN-INP NCs and irradiated with laser, f) PC3 cells incubated with Au-CALNN-INP NCs without laser irradiation, g) PC3 cells incubated with Au-CALNN-YIN NCs and irradiated with laser, and h) PC3 cells incubated with Au-CALNN-YIN NCs without laser irradiation. Scale bars: a,d) 10 μm; b,c,e,f) 3 μm; g,h) 1 μm.

120x179mm (300 x 300 DPI)